



# Obsidian Diffusion Dating by Secondary Ion Mass Spectrometry: A Test using Results from Mound 65, Chalco, Mexico

Lee R. Riciputi

*Chemical Sciences Division, Oak Ridge National Laboratory, P.O. Box 2008, Oak Ridge, TN 37831-6365, U.S.A.*

J. Michael Elam

*Department of Anthropology, 252 South Stadium Hall, University of Tennessee, Knoxville, TN 37996-0720, U.S.A.*

Lawrence M. Anovitz and David R. Cole

*Chemical Sciences Division, Bldg. 4500S, MS 6110, P.O. Box 2008, Oak Ridge National Laboratory, Oak Ridge, TN 37831-6110, U.S.A.*

*(Received 25 April 2000, revised manuscript accepted 17 April 2001)*

Secondary ion mass spectrometry (SIMS) was used to measure hydrogen and other elemental concentrations as a function of depth in ten obsidian artifacts (Pachuca Source), each with a well-constrained  $^{14}\text{C}$  date, from Mound 65, Chalco, Mexico. Hydrogen depth profiles for the different artifacts all display a characteristic S-shape, and increasing maximum hydrogen content in each profile and profile depths are well correlated with time. These data are used to investigate the potential use of Obsidian Diffusion Dating by SIMS (ODDSIMS) for both extrinsic and intrinsic dating of obsidian artifacts. Using “characteristic points” on the hydrogen profile (half-fall depth, inflection point depth), simple hydration rate equations were evaluated against time constraints provided by associated  $^{14}\text{C}$  dates. We demonstrate that neither the traditional OHD equation for depth ( $x$ ) as a function of the square root of time ( $t^{1/2}$ ) nor a linear function ( $t^1$ ) fit the data. Solving the more generalized  $t^n$  function provides an excellent fit between characteristic point depths and  $^{14}\text{C}$  dates (for  $n \approx 0.75$ ), and meets the constraint that at time equal to zero, the depth of the hydration profile must also be zero. However, this may be an average coefficient over the range of ages available, and may not accurately reflect rates at shorter or longer times. Using only two obsidian samples and their associated  $^{14}\text{C}$  dates, a calibration curve can be derived that provides ODDSIMS dates for the other pieces that are in excellent agreement with associated  $^{14}\text{C}$  dates, indicating that empirical application of the technique is potentially feasible, at least at individual sites.

The underlying processes governing hydrogen transport into the obsidian were also investigated by using finite difference modelling to reproduce the shape of the hydrogen depth profile. Excellent fits were obtained by assuming concentration-dependent diffusion, and dates that agree well with associated  $^{14}\text{C}$  dates can also be extracted from the finite difference profiles. Although considerable additional work needs to be done, the success of the finite difference modelling suggests that development of an independent, intrinsic ODDSIMS model may be possible.

© 2002 Elsevier Science Ltd. All rights reserved.

**Keywords:** OBSIDIAN, GLASS, HYDRATION, CHALCO, MOUND 65, DEPTH-PROFILE, ODDSIMS, DIFFUSION.

## Introduction

Of the various classes of artifacts recovered from Mesoamerican sites, perhaps none has as much potential scientific value as obsidian. This volcanic glass, intensively utilized by the cultures of ancient Mesoamerica to produce a variety of imple-

ments and ornaments, was distributed across the vast commercial networks that characterized much of pre-hispanic Mesoamerica, and the geographic distribution of different obsidians can be used to infer commercial and political connections (e.g., Charlton *et al.*, 1978; Santley *et al.*, 1986; Stark *et al.*, 1992; Elam *et al.*, 1994). Obsidian also has the potential to be used as a

chronometer by measuring the amount of water absorbed on the surface of obsidian artifacts. If practical, ancient exchange networks could be ordered temporally allowing study of Mesoamerican economies diachronically (Neff *et al.*, 1993; Elam *et al.*, 1994). Furthermore, dates resulting from obsidian chronometry could be used to develop and revise chronologies both locally and regionally (cf. Webster & Freter, 1990).

Obsidian Hydration Dating (OHD) was first proposed by Friedman & Smith (1960), who observed birefringent rims on obsidian artifacts under high magnification (approximately  $500\times$ ). Research subsequent to Friedman & Smith's original presentation has refined the method into two distinct techniques. The simplest, referred to as empirical rate dating, requires correlating the width of optically measured rims to independent chronometric data, such as  $^{14}\text{C}$  dates (e.g., Ambrose, 1976). The more complex and widely applied form, known as intrinsic-rate dating, requires experimentally determined rate constants and a measure of site temperature because it is theoretically a fully independent chronometric method (Friedman *et al.*, 1966; Friedman & Long, 1976; Michels *et al.*, 1983; Stevenson *et al.*, 1989, 1998). In spite of nearly 40 years of development and application, neither the intrinsic nor extrinsic methods has produced consistently reliable results. In some cases the results have so contradicted other well-established chronometric data that the utility of obsidian as a chronometer has been questioned (Braswell, 1992; Braswell *et al.*, 1996; Nichols & Charlton, 1996; Ridings, 1996; Anovitz *et al.*, 1999).

A recent study (Anovitz *et al.*, 1999) utilized secondary ion mass spectrometry (SIMS) to directly analyze the concentration of hydrogen as a function of depth through the hydration rim in a series of obsidian artifacts, and explored some of the assumptions underlying traditional optical OHD techniques. They documented a variety of problems, but focused on two primary difficulties with the traditional OHD method:

(a) The mathematical model utilized in intrinsic rate OHD

$$x^2 = Ate^{-E/RT} \quad (1)$$

where  $x$  is depth,  $A$  is a constant,  $E$  is the activation energy,  $R$  is the gas constant, and  $T$  is temperature does not correctly predict the shape of the water concentration depth profile actually measured by SIMS. This equation assumes that the hydration rim grows at a rate proportional to the square root of time, and that the diffusion coefficient is constant. The S-shaped hydrogen profiles measured by SIMS indicate that both assumptions are incorrect, and thus the rate equation that has been used in traditional OHD is incorrect.

(b) Traditional measurement techniques involve non-systematic errors arising from the inherent

imprecision of optical measurement. This is due to two factors, both of which are related to the physical limitations of optical microscopy. These factors, the wavelength of light and differential refractive indices, combine to produce the illusion of a sharp boundary between the hydrated and unhydrated portions of the glass (see Anovitz *et al.*, 1999 for a full discussion of these limitations). Consequently, optical measurement becomes a highly subjective, observer dependent exercise. Additionally, the wavelength of light imposes a theoretical precision limit of  $\pm 0.25\ \mu\text{m}$  on the rim width measurement. The net outcome is significant scatter, often on the order of hundreds if not thousands of years, in the predicted hydration dates.

Given these problems, Anovitz *et al.* (1999) concluded that it is unlikely that traditional optical OHD will ever produce consistently reliable chronometric results. At best, it may still be useful for relative dating or ordering of surface assemblages if age variations are large enough (Jones & Beck, 1990). More importantly, Anovitz *et al.* (1999) concluded that hydrated obsidian artifacts remain a potentially valuable source of chronometric data. However, for this potential to be realized, they indicated that a more rigorous analytical technique providing a direct measure of the hydration profile, and a correct understanding and model of the rates and mechanisms of obsidian hydration, would be required.

### Obsidian diffusion dating by secondary ion mass spectrometry (ODDSIMS)

In this report, we present the results of the first direct analyses (by SIMS) of hydration profiles from a set of chronometrically constrained obsidian artifacts from a single site. These samples span a 1000 year interval, and were recovered from Mound 65 at Chalco, Mexico (Hodges, (ed), *in press*). We will utilize the data from the Chalco artifacts to evaluate the potential of what we have termed ODDSIMS (Obsidian Diffusion Dating by Secondary Ion Mass Spectrometry) as a chronometric technique. As with traditional optical OHD, ODDSIMS shares the concept that the width of the hydration rim on obsidian can be used to date the amount of time elapsed between the manufacture of an obsidian artifact and the present. However, the SIMS analyses yield detailed data on the concentration of hydrogen (and other elements) as a function of depth through the hydrated obsidian rim, information that can not be obtained optically. This information provides a quantitative measure of the chemical processes occurring in the hydration rim, allowing more direct investigation and mathematical modelling of diffusion kinetics. We will use the data in two ways.

Firstly, "characteristic points", representative of the hydration depth, can be compared with associated  $^{14}\text{C}$  dates for multiple artifacts. The  $^{14}\text{C}$  ages and

“characteristic points” can be regressed using various simple rate equations. If a good fit is obtained using a rate equation, the potential of applying an empirical calibration to use hydration depths as a chronometer can be evaluated. Secondly, the detailed shape of the hydration profiles can be used to investigate actual hydration mechanisms, processes, and rates. This is done by taking fundamental diffusion equations and using finite difference modelling to attempt to reproduce (1) the shape of the hydration profiles, and (2) how the shapes and depths vary as a function of time. This modelling yields valuable information about the nature of transport mechanisms (e.g., how the diffusion rate varies as a function of water content) and can provide a generalized rate equation. If equations can be developed that provide a good fit between measured and predicted hydration profiles, it suggests that the hydration processes are systematic. Although full development of such an approach will have to wait until the completion of experiments designed expressly to extract rate information, successful modelling will provide the basis for developing an accurate, independent chronometric methodology.

### Analysed Samples and Archaeological Setting

To carry out a rigorous investigation of the potential of ODDSIMS utilizing obsidian artifacts, it is crucial to obtain samples from a single site that (1) are from secure contexts, (2) span a significant temporal period, and (3) have good independently determined ages. As described below, obsidian samples recovered from the Chalco, Mexico site provide an excellent suite of material.

The ancient city-state of Chalco was located along the southeastern shore of Lake Chalco in the Basin of Mexico (Figure 1). Little is known of the Classic (200–750 CE) period of settlement, but during the Early Postclassic (750–1200 CE) Chalco grew to be the principal city of the Chalca, and was one of 40 major urban centres in the Basin of Mexico during the Late Postclassic (~1200–1521 CE) (Sanders *et al.*, 1979; Parsons *et al.*, 1982; Hodge, *in press*). The artifacts analysed for this report were recovered during the 1992 excavation of Mound 65 (formerly known as site Ch-ET-27), directed by the late Mary Hodge. Previous work at the site indicated the presence of both Early Toltec (Early Postclassic) and Aztec occupations (Parsons *et al.*, 1982; Hodge, *in press*). The excavation phase of the project involved two units, designated “A” and “B”. Both excavation units encompassed a surface area of 2 × 4 m<sup>2</sup> and were hand excavated according to natural stratigraphy. As illustrated in Figure 1, Unit A was excavated to a depth of 2.33 m revealing a total of 20 cultural levels, and Unit B was excavated to a depth of 2.37 m revealing 16 distinct cultural levels.

### *Chronology at Mound 65: Ceramics*

Combined excavation and surface collection recovered a total of 990 kg of potsherds. Analysis identified a total of 6660 diagnostic rim sherds, including 2588 recovered by surface collection (Hodge, *in press*). Analysis of the diagnostic rims was undertaken to determine the degree of local variability in the ceramic assemblage at Mound 65 and to fit the site into the regional Basin of Mexico chronology (Hodge, *in press*). The analysis revealed two major occupations. The first dates to the Epiclassic (also known as the Early Toltec period or the Coyotlatelco phase) and spans the period 750–950 CE (Sanders *et al.*, 1979). The second spans the Aztec period, encompassing all three sub-periods numbered Aztec I–III (Sanders *et al.*, 1979) covering the epoch 1150–1519 CE. This indicates a hiatus (abandonment) at Mound 65 of roughly 200 years.

A detailed review of the results of the ceramic analysis is beyond the scope of this report, but Table 1 presents a summary of the counts and percents of eight important pottery types recovered from Mound 65 for levels that produced an obsidian artifact analysed for this report. Although more than 60 types of vessels were identified during the analysis (Hodge, *in press*), these eight types are considered to be excellent regional horizon markers and thus link Mound 65 to the wider chronology of the Basin of Mexico. Types indicative of the Epiclassic include Red-on-Buff (the hallmark Coyotlatelco phase horizon marker), Red-on-Cream, Brown Incised and Brown Carved. Types considered datable to the Aztec periods include Aztec Black-on-Orange (variants I, II & III; once again, ideal horizon markers) and Black-on-Red. Table 1 clearly depicts the dichotomy in occupation noted during the ceramic analysis. The Epiclassic occupation at Mound 65 is seen primarily in the deepest levels of Unit A. Unit B mainly reflects the Aztec period occupation. Note that the absence of values for the two features (associated with obsidian samples CHO047 and CHO081) reflects the fact that these are burials that produced intact vessels.

### *Chronology of Mound 65: Radiocarbon Assay*

Mound 65 was relatively rich in samples suitable for radiocarbon dating, especially charcoal and other carbonized plant remains, but also bone. All of the collected samples were submitted to Beta Analytic for analysis. Table 2 presents the radiocarbon dates for the levels that yielded obsidian artifacts discussed in this report. The radiocarbon dates indicated occupations at Mound 65 dating from 400–1620 CE (based on 2 sigma calibrated ranges) with a hiatus occurring roughly from 900–1100 CE. One significant aspect of the radiocarbon assay is the indication that the Epiclassic period begins substantially earlier than previously believed, but further analysis is needed from other sites in the southern Basin to substantiate this possibility. Agreement between the ceramic data and the radiocarbon

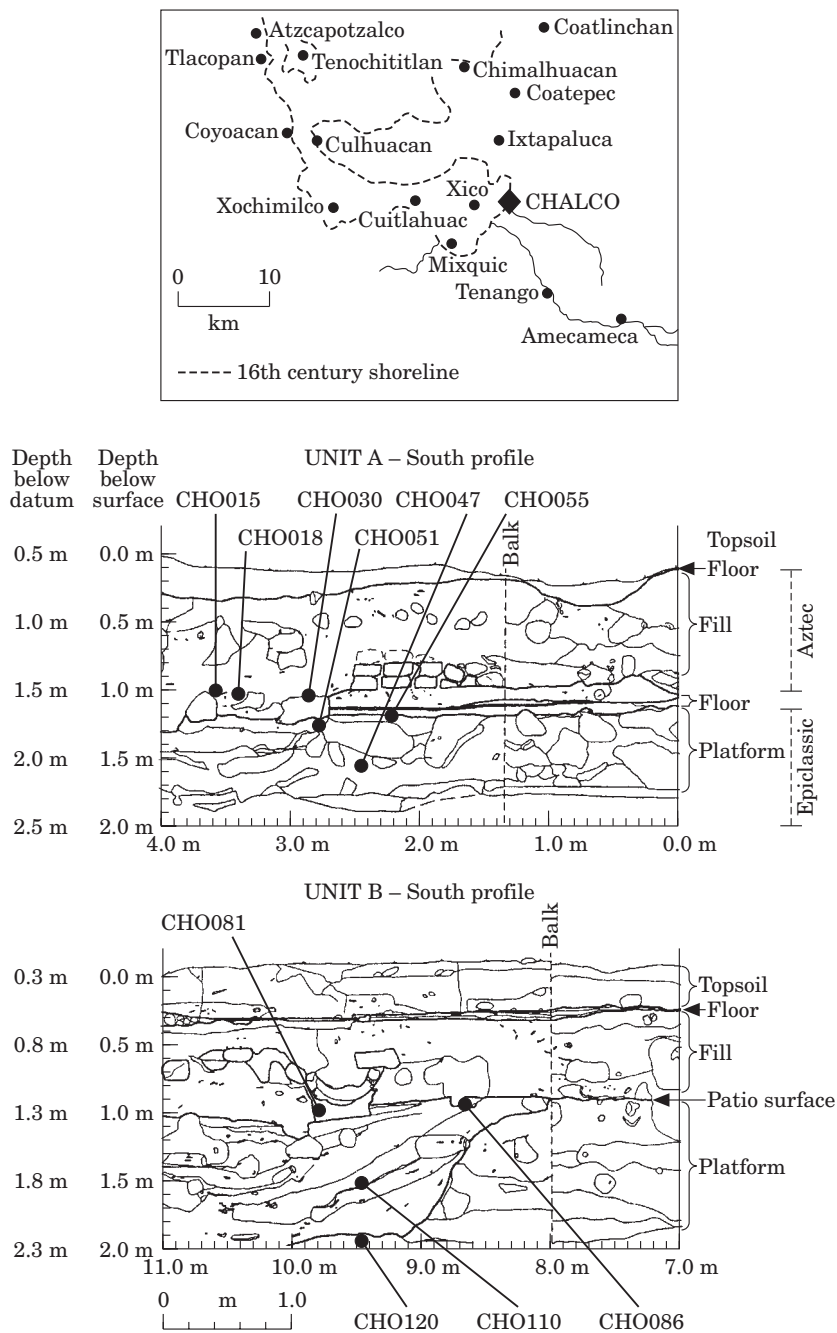


Figure 1. Chalco location and cross section.

dates is good, suggesting that the ceramic analysis was correct in identifying a hiatus. Although noteworthy, the reasons for this hiatus, during the time when the Toltecs ruled the Basin of Mexico, have yet to be discovered. With the exception of a single effigy-footed Red-on-Cream dish with a stamped base recovered from a grave (Feature 2, Unit A) which has formal attributes that are suggestive of Mazapan pottery, no diagnostic ceramics datable to this period were recovered. Significantly, no other Late Toltec types, such as Graphite-on-Orange, were recovered from the burial

and the rest of the vessels were clearly identifiable Epiclassic types. Furthermore, the radiocarbon date from the burial (intercept=640 CE) supports Epiclassic date. A good possibility is that this interment occurred late in the Epiclassic occupation, perhaps just prior to the Mounds abandonment.

*The Obsidian Hydration Dating Project at Mound 65*

A total of 120 obsidian artifacts, mostly prismatic blades, were selected for provenience analysis and

Table 1. Summary of pottery associations at Chalco

Unit/ level	Obsidian sample CHO***	R/Bf	R/Cm	Br-in	Br-cv	Az I	Az II	Az III	Bl/Rd	Total	% Aztec
A, 8A&C	015, 018	4	2	2	1	8	0	0	4	21	67.1
A, F.2, Br	047	nr	nr	nr	nr	nr	nr	nr	nr	nr	nr
A, 12	030	7	1	2	0	1	0	0	0	11	11.1
A, 15	051	4	1	0	1	0	0	0	0	6	0
A, 17	055	3	0	0	0	0	0	0	0	3	0
B, 9, E	086	40	6	7	1	28	1	1	127	216	75
B, F.2	081	nr	nr	nr	nr	nr	nr	nr	nr	nr	nr
B, 14, EW	110	11	2	4	0	14	0	0	29	62	72.6
B, 16, S	120	34	0	3	0	15	0	0	99	156	76.3

Associated ceramic counts and summary percents of eight horizon markers by level for the obsidian artifacts. The nr for the two features reflects that these are burials that produced intact vessels rather than sherds. With the exception of one possible piece of Late Toltec pottery, the A, F.2 burial produced Epiclassic material. The B, F.2 burial produced Aztec pottery. Type abbreviations are: R/Bf—Red on Buff; R/Cm—Red on Cream; Br-in—Brown incised; Br-cv—Brown carved; Az I—Aztec I; Az II—Aztec II; Az III—Aztec III; Bl/Rd—Black on Red.

Table 2. Summary of  $^{14}\text{C}$  dates on analyzed Chalco samples

Obsidian sample	$^{14}\text{C}$ assay ID#	Sample level	$^{14}\text{C}$ age (years BP)	$1\sigma$	Uncal. $^{14}\text{C}$ date (CE)	Calibrated $^{14}\text{C}$ date (CE)	Calibrated range $-1\sigma$ (lower)	Calibrated range $+1\sigma$ (upper)	Calibrated range $-2\sigma$ (lower)	Calibrated range $+2\sigma$ (upper)	Median intercept date (CE)
CHO110	BETA-57758	Unit B, L.14	430	60	1520	1450	1430	1500	1410	1640	1525
CHO086	BETA-57754	Unit B, L.9	580	60	1370	1400	1310	1360	1290	1440	1365
CHO081	BETA-57756	Unit B, L9f2	610	80	1340	1320	1290	1420	1270	1440	1355
CHO120	BETA-57757	Unit B, L16	760	70	1190	1270	1230	1290	1170	1320	1245
CHO015	BETA-57748	Unit A, L8	850	90	1100	1210	1110	1270	1010	1300	1155
CHO018	BETA-57748	Unit A, L8	850	90	1100	1210	1110	1270	1010	1300	1155
CHO047	BETA-57753	Unit A, L13-14	1420	110	530	640	550	690	420	870	645
CHO055	BETA-57751	Unit A, L.17	1480	100	470	610	520	660	400	720	560
CHO051	BETA-58555	Unit A, L.15	1470	90	480	620	540	660	410	710	560
CHO030	BETA-57750	Unit A, L.12	1350	70	600	670	640	720	600	820	710

The uncalibrated date (uncal.  $^{14}\text{C}$  date) is obtained by subtracting the uncalibrated age from 1950. The calibrated date represents the direct intercept obtained during age calibration. The calibrated median intercept (date) is derived using the equation:

$$\text{Md}_{\text{Cal}} = (\text{R}_L - \text{R}_U) / 2 - \text{R}_U$$

where  $\text{Md}_{\text{Cal}}$  = the calibrated median intercept,  $\text{R}_L$  = the lower calibrated range value ( $-1\sigma$ ), and  $\text{R}_U$  = the upper calibrated range value ( $+1\sigma$ ).

dating (Elam *et al.*, in press). The samples were evenly divided between the two excavation units. Many of the selected artifacts came from levels that had produced suitable materials for radiocarbon assay, allowing the artifacts to be independently dated (see Hodge; Elam; Elam *et al.*, all in press). The provenience analyses indicate the predominance of two obsidian sources in the assemblage, Pachuca (or Sierra de las Navajas) and Otumba, along with the minor occurrence of obsidian obtained from three other sources (Ucareo, Zaragoza and Paredon; see Elam *et al.*, in press). Artifacts made from either obsidian are useful for standard intrinsic-rate OHD since induction experiments have been undertaken and rate constants are available (see Elam 1993). The OHD program was undertaken to (1) increase the number of chronometric determinations obtained from the site to develop a fine-grained absolute chronology, and (2) to obtain better temporal resolution of the changes in obsidian procurement

patterns observed through the levels at Mound 65. The large amount of obsidian recovered from Mound 65, often from radiocarbon dated levels, made the option of OHD even more attractive since independent temporal controls were available.

Rim measurements made at two established labs experienced in intrinsic rate OHD, referred to as Labs A and B\*, differ significantly throughout the entire set of 120 artifacts (Table 3). In accordance with established OHD protocol, four pairs of temperature and humidity cells were prepared by Lab B. The cells were buried in Mound 65 for a period of one year (1994–1995). Burial depths ranged from 0.25–2.00 m. Results of these measurements are presented in Table 4. Dates calculated by Lab A are based on an EHT (estimated

\*In the interest of fairness and to emphasize that our research is not intended as an attack on either the labs or the individuals who work in them, we have chosen to designate the laboratories where the OHD analyses were performed by letters rather than by name.

Table 3. Summary of measured parameters in Chalco samples

Obsidian sample	Maximum wt% H <sub>2</sub> O	Fitted surface wt% H <sub>2</sub> O	SIMS half-fall depth (µm)	SIMS inflection depth (µm)	Lab A OHD Depth (µm)	Lab B OHD Depth (µm)	Lab A OHD date (CE)	Lab B OHD date (CE)
CHO110	8.18	9.0	1.97	2.18	2.53	2.28	1108	794
CHO110	8.20	9.1	2.11	2.30	2.53	2.28	1108	794
CHO086	8.36	8.9	2.08	2.21	2.49	2.34	1137	768
CHO081	8.16	9.0	2.19	2.38	2.52	2.53	1113	550
CHO081	8.36	9.0	2.28	2.44	2.52	2.53	1113	550
CHO120	8.58	8.8	2.23	2.41	2.85	2.51	866	585
CHO015	8.88	9.4	2.41	2.63	2.59	2.58	1062	613
CHO018	8.92	9.1	2.48	2.85	2.76	2.86	937	149
CHO047	10.00	10.2	3.79	4.19	3.56	3.43	228	- 551
CHO055	10.09	10.0	3.81	4.25	3.60	3.56	194	- 805
CHO051	9.95	9.85	4.00	4.40	4.29	3.71	- 576	- 984
CHO051	10.10		3.87		4.29	3.71	- 576	- 984
CHO030	9.32	9.9	2.69	2.91	2.93	2.78	802	343

OHD dates for Lab A calculated from measured depths using an EHT of 20°C and a Rh of 100%.

OHD dates for Lab B calculated from measured depths using an EHT of 19.4°C and an Rh of 97.5%.

Note that a “-” sign before an OHD date indicates BCE.

hydration temperature) of 20°C and a Rh (relative humidity) of 100%, and those of Lab B are based on a EHT of 19.4°C and 97.5% Rh. The Lab A value represents the upper range of recorded temperatures (see Table 4), whereas the values used by Lab B were the averages of the cell values. The dates calculated using the two data sets disagree, and neither set of measurements produced acceptable results when compared to either <sup>14</sup>C dates or ceramic assemblages. Using the same set of temperature and humidity values to recalculate the dates does not improve the agreement between the two labs. Use of ambient air temperature data from Chalco (Garcia M, 1987) and the conversion equation of Lee (1969) results in an EHT of 16.3°C, substantially lower than that obtained by direct measurement. Dates based on this value are even more unacceptable than the ones based on the temperature-humidity cells. Regardless of which EHT and Rh values are used, the results are discordant with the radiocarbon assays and ceramic data. In fact, the results from the OHD program are so at odds (in some cases by thousands of years) with the other

chronological indicators that they could not be used and were excluded from the excavation report.

The sample set from Mound 65 is ideal for demonstrating both the potential of obsidian as a chronometer and the advantages of the ODDSIMS method. The attractiveness of this sample set lies in the contextual integrity of Mound 65 (as demonstrated by the careful excavation of Dr Hodge), the fact that obsidian dating was a primary focus of the excavation, and by the independent chronological control provided by the detailed radiocarbon sequence. To demonstrate the advantages of the ODDSIMS approach, we selected 10 artifacts manufactured from Pachuca obsidian (Table 1) from the original OHD sample set, based on having an associated <sup>14</sup>C date and to span the range of occupation at Chalco.

## Analytical Methods

### SIMS analysis

*Sample preparation.* To prepare samples for ODDSIMS analysis, small cross-sections (approximately 1 mm wide) were cut from each of the obsidian artifacts. The ventral face was typically chosen for analysis because it is the flattest and broadest surface of a typical prismatic blade. Five to six holes were drilled in 1 in diameter,  $\frac{3}{8}$  in thick aluminum disks. Epoxy was used to mount the obsidian samples in these holes with the hydrated surface exposed. A sample of freshly polished Pachuca obsidian was also mounted in each disk to (a) ensure the availability of a flat surface to aid with calibrating sputter depths (see discussion below) and (b) provide an internal standard. The finished disks were coated with a thin layer of gold to provide surface conductivity. To minimize the presence of adsorbed water, samples were baked at 45°C for

Table 4. Summary of Ambrose cell measurements at the Chalco site

Cell #	Depth below mound surface (cm)	EHT (°C)	Rh
94-1			
94-2	25	20.3	95%
94-3	50		
94-4	50	19.1	97%
94-5	100		
94-6	100	18.9	98%
94-7	200		
94-8	200	19.3	100%

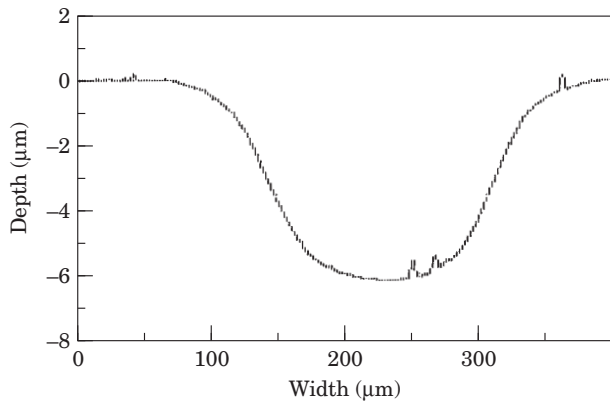


Figure 2. Shape of typical crater sputtered in obsidian during a SIMS analysis. Only ions from the centre  $\sim 30 \mu\text{m}$  of the crater (flat area) are analysed. Note  $\sim 40:1$  vertical exaggeration.

12–18 h prior to analysis before introduction into the vacuum system of the mass spectrometer, which occurred a minimum of 12 h before analysis. Experiments discussed below indicate that these steps result in minimization of adsorbed hydrogen prior to analysis.

*Analytical conditions.* The distribution of hydrogen (and other elements including O, Na, Mg, Al, K, Ca, Fe) as a function of depth (depth-profiles) was measured using a Cameca 4f secondary ion mass spectrometer. The SIMS technique utilizes a focused, mass selected beam of primary ions accelerated to sputter the surface of the obsidian. For these analyses, negatively-charged,  $^{16}\text{O}$  primary ions were accelerated at 12.5 keV. The primary beam, with a diameter of  $\sim 50 \mu\text{m}$  and a current of 130 nA, was rastered over an area of  $150 \times 150 \mu\text{m}^2$  to produce a well-shaped crater with a flat bottom (Figure 2). The primary ion beam slowly sputters into the sample surface (a few atom layers at a time; the sputter rate was  $\sim 2.2 \mu\text{m/h}$ ). By monitoring changes in the intensity of secondary ions ejected from the sample surface as a function of time, a spatially resolved profile of changing elemental concentrations as a function of depth is obtained. Positively charged secondary ions with  $80 \pm 20 \text{ eV}$  of excess kinetic energy were analysed. Use of the  $150 \mu\text{m}$  diameter transfer lens and a  $400 \mu\text{m}$  diameter field aperture restricts transmission so that only ions from the central  $33 \mu\text{m}$  of the sputter crater are transmitted through the secondary mass spectrometer. Selected masses were analysed by cycling the secondary ion magnet through the masses of interest. Secondary ion signals were monitored using an electron multiplier, with count times of 1–3 s per cycle per element of interest. Ion yields of the different elements are directly correlated with concentration, and were calibrated using a suite of glass standards. The intensity of  $^{30}\text{Si}$  was used as a reference species to correct for variations in secondary ion intensities due to changes in primary ion beam intensity between different analyses.

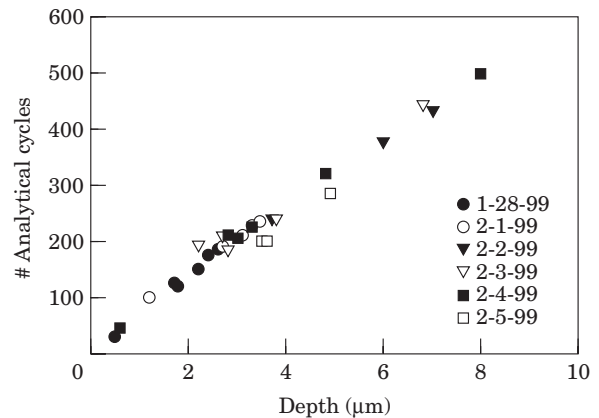


Figure 3. Plot of crater depth as a function of number of analytical cycles on Pachuca obsidian. Data obtained over a 2 week period. All analyses conducted using a 130 nA primary ion beam rastered over a  $150 \times 150 \mu\text{m}^2$  area. Analytical cycles are directly correlated to time of sputtering (100 cycles  $\sim 45 \text{ min}$ ).

*Measurement of sputter crater depth.* One critical step in the analytical procedure is measurement of crater depth, because without this information, the time-series elemental distributions obtained during the SIMS analysis can not be depth-calibrated. Crater depths were measured using an Tencor Alpha-Step 200 profilometer. For most samples, the craters are very regular in shape with wide, flat, bottoms, indicating that depth resolution was optimized during the analysis (Figure 2). Repeated depth measurement on craters sputtered on flat samples indicates that reproducibility of the depth measurement is better than 3%.

For some samples, fractures, excessive curvature, and other surface imperfections make determination of the sputter depth using the surface profilometer much less certain. Fortunately, if the primary beam current is kept constant, the sputter rate is also constant. As previously noted, a flat piece of polished Pachuca obsidian was mounted in every sample block to ensure the presence of a flat surface. Craters were routinely sputtered into this material to provide a check on the sputter rate. Crater depth versus sputter time (in magnetic cycles) is plotted in Figure 3 for both the polished samples and the unknowns. The correlation between sputter rate and crater depth is linear and very reproducible, even over a span of several days. Using this calibration, the sputter depth can be estimated accurately even on samples where direct profilometer measurements are difficult.

*Effects of vacuum on the hydrated rim.* One potential analytical concern was possible dehydration of the obsidian rim due to prolonged exposure to the high vacuum conditions in the mass spectrometer (typically  $0.5$  to  $2 \times 10^{-9}$  torr). To determine the magnitude of this effect, a sample of hydrated Pachuca obsidian (CH0095) was put into the mass spectrometer, and profiles periodically measured at times after first

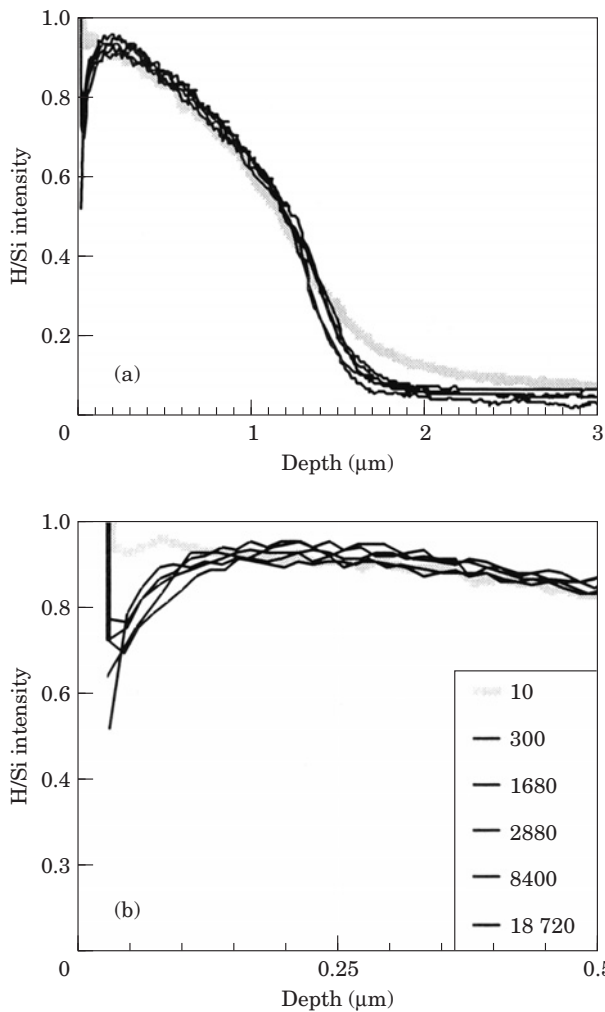


Figure 4. Results of experiments testing the effect of prolonged exposure to high vacuum ( $\sim 1 \times 10^{-9}$  torr) in the mass spectrometer on hydration profiles obtained from sample CHO095. Figure A illustrates results for the whole profile; Figure B is a blow-up illustrating only the first 0.5  $\mu\text{m}$  of the profile. Captions give the times the analyses started after exposure to high vacuum in minutes. All analyses except the analysis started 10 minutes after exposure to vacuum are essentially identical.

exposure to vacuum ranging from 10 min to over 300 h. The results of this experiment are summarized in Figures 4a and b. Several conclusions can be drawn from this set of experiments. The only significant changes in concentration as a function of vacuum exposure time occur in the first 0.1  $\mu\text{m}$ , and in the tail of the profile. The portions of the profiles between these extremes are consistent and reproducible, indicating that there is no significant dehydration of the samples due to vacuum effects over a period of nearly two weeks. Sample blocks are typically exposed to vacuum for less than 50 h, indicating that dehydration should not be a concern. The similarity of these profiles for multiple analyses over a 2 week period also demonstrates the high degree of reproducibility in SIMS analysis of the profile. The effects of adsorbed water

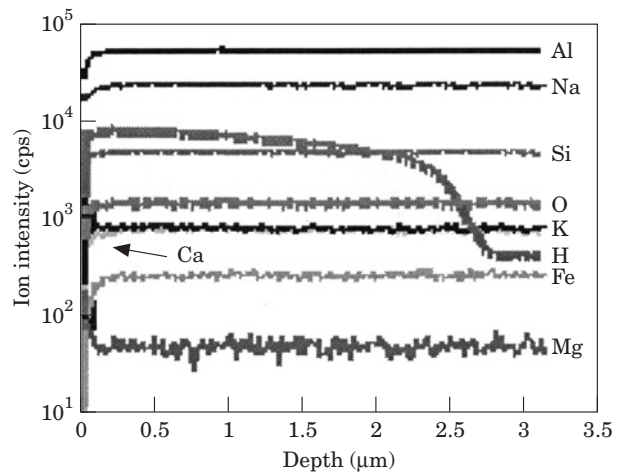


Figure 5. Profile illustrating the variation in ion intensities (directly correlated to concentration) as a function of depth in a typical profile (CHO120).

can be assessed by examining the first analysis, conducted immediately after the sample was exposed to vacuum. Although the overall hydrogen profile is similar to that in other samples, both surface and baseline levels of hydrogen are significantly elevated due to higher hydrogen background. However, the analysis started 5 h after exposure to vacuum is similar to all other profiles, indicating that the minimum hydrogen background had been reached by this time.

## Analytical Results

### Measured SIMS profiles

Profiles were measured on the ten selected artifacts of Pachuca obsidian from Chalco with associated  $^{14}\text{C}$  dates ranging from 610–1450 CE. Multiple measurements were performed on three samples. A representative example of a profile through a hydrated Pachuca rim for all the analyzed elements (H, O, Na, Mg, Al, K, Ca, Fe) is shown in Figure 5. Typical profiles begin with a near-surface area in which the secondary ion intensities vary rapidly as equilibrium sputtering conditions are established, followed by a narrow region in the outer 0.1–0.3  $\mu\text{m}$  where, in most samples, hydrogen and sodium count rates increase, and potassium count rates decrease. After  $\sim 0.3$   $\mu\text{m}$  depth, the secondary ion intensities of most elements become essentially constant throughout the remainder of the profile. In contrast, the hydrogen profile contains a broad region of slowly decreasing intensities through the major portion of the profile. This is followed by a relatively narrow zone, approximately 0.5  $\mu\text{m}$  wide, where the hydrogen count rate decreases rapidly, before the hydrogen profile flattens to baseline values. This profile is typical of that measured in obsidians from a variety of settings and, as discussed by Anovitz *et al.* (1999), indicates that the intrinsic OHD equations are an

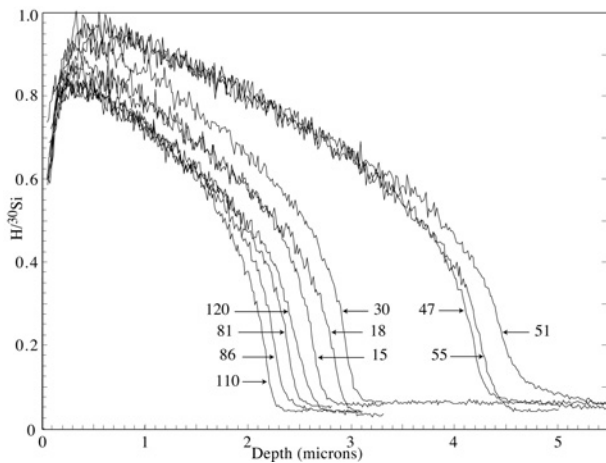


Figure 6. Summary of hydrogen depth profiles in all samples. Profiles are labelled using abbreviated sample numbers (no CHO).

incorrect model of the actual hydration process. One additional important observation is that the oxygen concentration appears to be constant throughout the entire depth profile, which, as discussed below, has important ramifications for the mechanism of hydration.

Depth profiles of hydrogen content for all samples are illustrated in Figure 6. The hydrogen profiles have very similar shapes, and the depth of the profile is systematically correlated with age. In addition, although not readily apparent on this plot, the maximum hydrogen content in the rim appears to be correlated with increasing age. This relationship is better illustrated in Figure 7.

## Extracting Age Information—Empirical Methods

### Characteristic points

There is now overwhelming evidence that the traditional OHD equation based on equation (1), a  $t^{1/2}$  relationship, is incorrect (e.g., Anovitz *et al.*, 1999). Two new observations from Chalco suggest that the hydration process may be far more complex than the simple self-diffusion assumed in traditional OHD. The first is that, within analytical precision ( $<0.1$  wt %), the oxygen content is constant across the hydration rim, an unexpected result. The lack of a concomitant increase in oxygen associated with elevated hydrogen contents in the hydrated rim implies that only hydrogen is moving into the sample, and that a more accurate term for the process might be hydrogenation rather than hydration. The second important observation is that the maximum hydrogen concentration in the hydrated rims of different obsidians is not constant, but is positively correlated with increasing age. Both of these results suggest that the “hydration” process may actually be comprised of several distinct mechanisms,

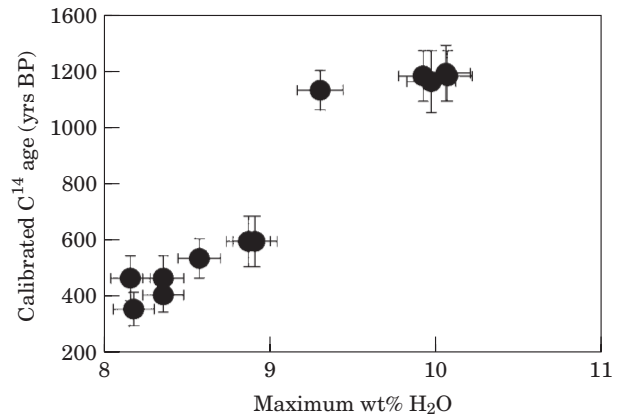


Figure 7. Plot of the maximum water content obtained in each profile as a function of  $^{14}\text{C}$  age. Error bars are 1 standard deviation.

each with different rate dependencies, which may correlate with a number of environmental and chemical variables. If so, this will add significant complexity to any final model of obsidian hydration. We have an ongoing experimental glass hydration program whose results will allow testing of theoretical models of obsidian hydration. However, at present, an accurate theoretical hydration model is not available.

Without a well-constrained intrinsic hydration model, it is impossible to independently extract dates from the hydration profiles presented here, because there is no way to calibrate the hydration rate. However, by utilizing associated  $^{14}\text{C}$  dates, it is possible to investigate the relationship between the hydration profiles and the age of the obsidian. If the information contained in the hydrogen depth profile can be successfully correlated with  $^{14}\text{C}$  ages, this approach can be used to develop an interim empirical method of dating obsidian utilizing ODDSIMS. Such a result will demonstrate that development of an intrinsic model may be feasible.

Data presented in Figure 6 demonstrate that the shape of the hydrogen profile is very consistent in all the samples. Moreover, the depths of the profiles are positively correlated with age, indicating that the hydration process is temporally sensitive. Together, these factors indicate that age estimates can be derived from analysis of these data. The most basic, empirical approach involves developing a simplified representation of the overall profile using well defined “characteristic points”. These characteristic point depths can be calibrated to the radiocarbon assays (either through regression analysis or two point anchoring) using simple rate equations and age estimates derived. The goodness of fit between the hydration ages and the  $^{14}\text{C}$  ages for a series of samples provides an excellent check of whether empirical hydration dating is feasible.

The “characteristic point” method for deriving age estimates requires that the depth-profile be defined as a function of a single depth. While there are a number of

different options that could be used for defining a “characteristic point”, we will only discuss results based on two different mathematical formulations. The first technique is based on the depth at which the hydrogen concentration is halfway between the maximum concentration and the baseline concentration—the *half-fall depth*. This measurement provides a link between the SIMS depth and the purported depth measured using traditional optical methods. The second technique is based on finding the *inflection point*, the depth at which the slope of the depth-profile stops decreasing by obtaining the first derivative of the hydration curve (note that this approach is similar to that used in describing paramagnetic resonance peaks used in electron spin resonance dating (e.g., Geyh & Schliecher, 1990; Aitken, 1997; Grun, 1997).

*Characteristic point 1—half-fall depth.* Anovitz *et al.* (1999) noted that the standard equation used in OHD is based on modelling the distance at which the concentration of water was approximately half the difference between the surface and background concentrations for an error function-type solution to the diffusion equation. The SIMS profile data conclusively demonstrated that such an equation does not, in fact, describe the actual concentration versus depth profile for water in hydrated obsidians. However, the approach can be generalized to the SIMS results using the depth at which the concentration is the average of the background value and the maximum concentration analysed near the obsidian surface.

The relation between half-fall depth and associated  $^{14}\text{C}$  ages is plotted in Figure 8a (for the  $t^1$  function) and Figure 8b (for the  $t^{1/2}$  function assumed in intrinsic rate OHD). As can be seen, a systematic relationship exists between age and depth for all but sample CH0030 (which may have an uncertain context, as discussed below). Consideration of these two plots indicates that although both  $t^{1/2}$  and  $t^1$  age functions result in systematic correlations between the  $^{14}\text{C}$  age and the measured hydration profile, neither relationship is strictly linear, and projection of either line to zero time does not result in a half-fall depth of zero. Non-linearity on a plot of log half-fall depth against the log of the sample age (Figure 8c) confirms that neither equation is an adequate model of the apparently complex hydration process.

*Characteristic point 2—inflection point.* The inflection point occurs at the depth where the hydration curve changes from being concave downward (exclusive of the near-surface region) to concave upward as the background value is approached. It is a minimum in the first derivative, and a zero in the second derivative of the concentration-versus-depth curve. Figure 9 illustrates the first derivative of the hydration profile for one sample (CHO47) as an example, demonstrating that the location of the inflection point is clearly

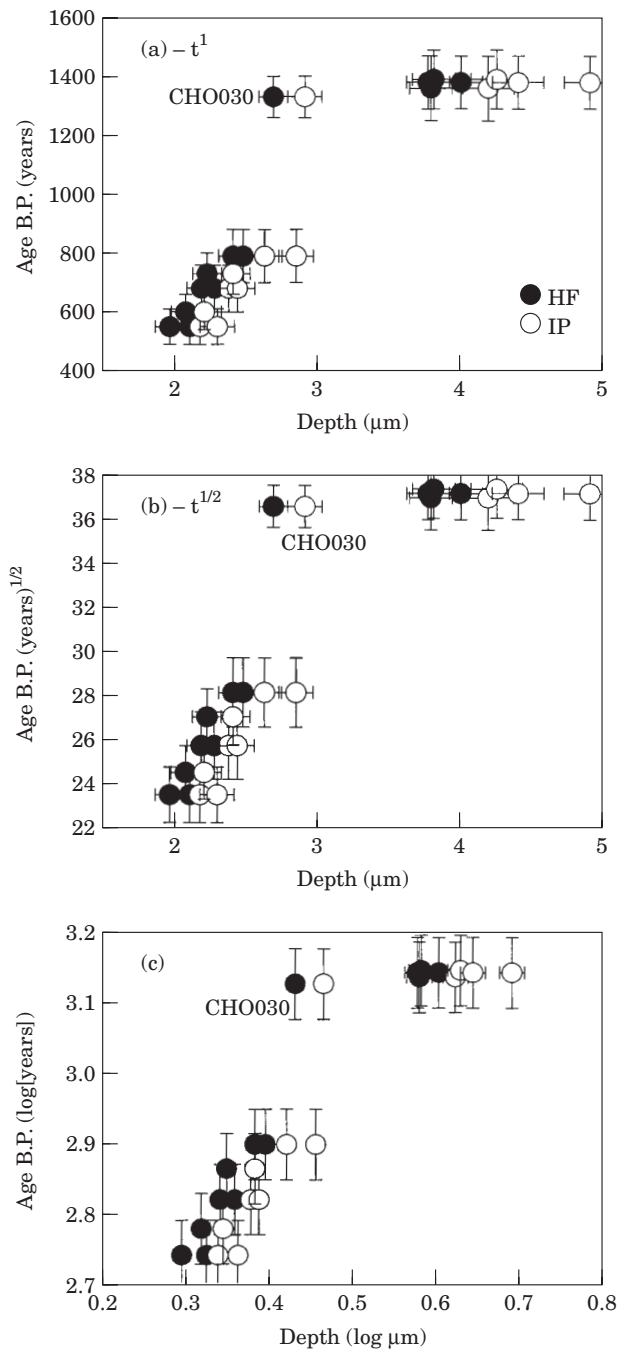


Figure 8. Plots of characteristic point depths against associated  $^{14}\text{C}$  ages. (A)– $t^1$  time relation, (B)– $t^{1/2}$  time relation, (C)–log depth versus log time. HF–half-fall depth, IP–Inflection point depth. Error bars are 1 standard deviation.

identified. While the initial curve used to calculate Figure 9 has, in this case, been smoothed with a three-point running average to reduce noise, this procedure has no effect on the inflection point location. The first derivative of the profile was calculated using the average of the forward difference and backward difference as:

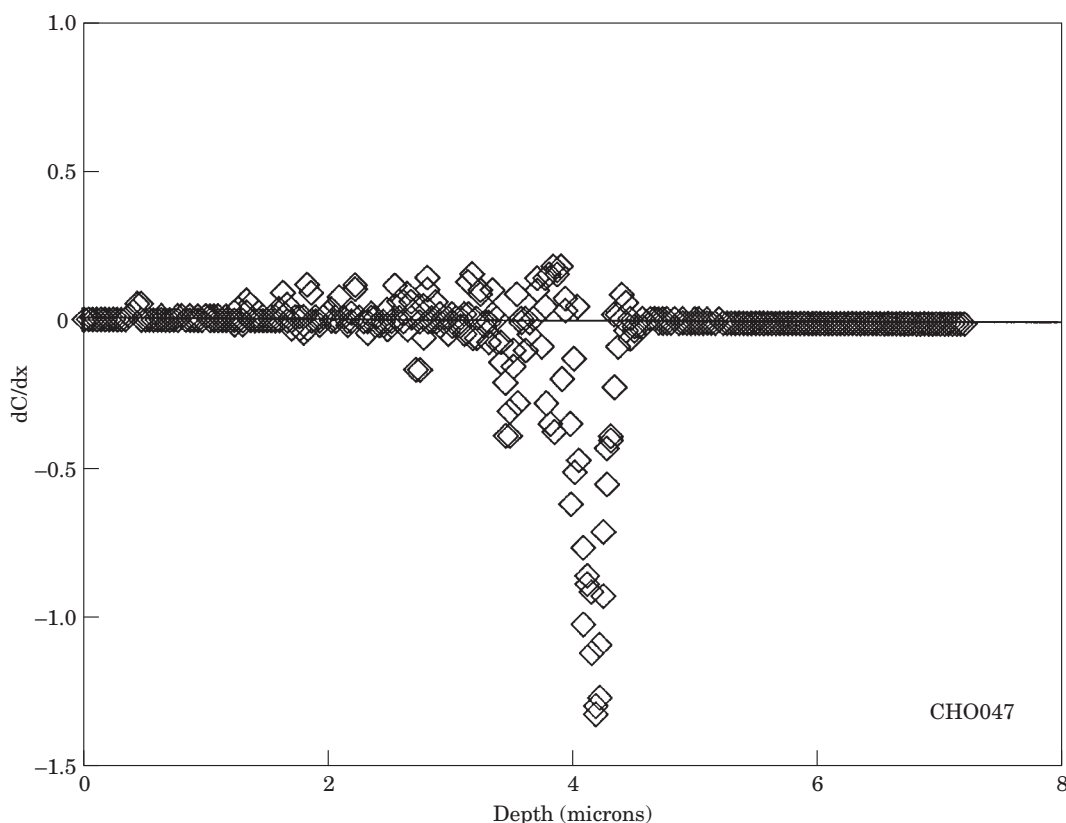


Figure 9. The first derivative of the concentration as a function of depth for sample CHO047. The inflection point is located at the minimum of the negative spike near 4  $\mu\text{m}$  depth.

$$\left(\frac{\partial C}{\partial x}\right)_i = \frac{\left[\left(\frac{C_{i+1} - C_i}{x_{i+1} - x_i}\right) + \left(\frac{C_i - C_{i-1}}{x_i - x_{i-1}}\right)\right]}{2} \quad (2)$$

where the subscripts refer to the depth step,  $C$  is the concentration, and  $x$  is the distance from the surface. The resultant values for each sample are listed in Table 3, and the relation between the inflection point depths and associated calibrated  $^{14}\text{C}$  ages is plotted in Figure 8a and b (for a  $t^1$  and  $t^{1/2}$  relationship, respectively). As can be seen, both relationships appear reasonably linear, but neither projects to zero distance at zero time.

*Hydration dating using characteristic point models.* In evaluating the characteristic point techniques we will consider three rate dependencies, including Model 1, the intrinsic OHD equation with a  $t^{1/2}$  relation ( $x$ =distance and  $t$ =time):

$$t^{1/2} = Dx \quad (3)$$

Model 2, a linear dependence, which has been advocated by Meighan & Haynes (1970) and Garcia-Barcelona (1989)

$$t^1 = Dx \quad (4)$$

and Model 3, the general exponential equation where  $n$  is a best-fit coefficient.

$$t^n = Dx \quad (5)$$

To evaluate these equations, the measured half-fall distances and inflection points were regressed against the associated  $^{14}\text{C}$  dates using the appropriate forms of the equations for all samples except CHO030. Regressing the measured half-fall depths against the  $^{14}\text{C}$  age data results in an excellent fit for all three models (Figure 10a). However, a major problem is clearly illustrated. Projection of the  $t^{1/2}$  fit to zero time results in a large “negative” depth; projection of the  $t^1$  fit to time zero results in a positive rim width. Neither of these results is realistic: at time equal to zero, the hydration depth ( $x$ ) must also be zero.

Attempts to fit the depth-age relation using the  $t^1$  and  $t^{1/2}$  equations (3 and 4) with the realistic constraint that at time equal to zero, hydration depths must be zero, are much less satisfactory. The  $t^{1/2}$  model calculates hydration depths that are greater than those measured on the younger samples, and depths that are shallower than measured for the older samples (Figure 10b). The opposite is observed with the  $t^1$  model. Use of either of these models results in systematic discrepancies between the measured  $^{14}\text{C}$  age and predicted

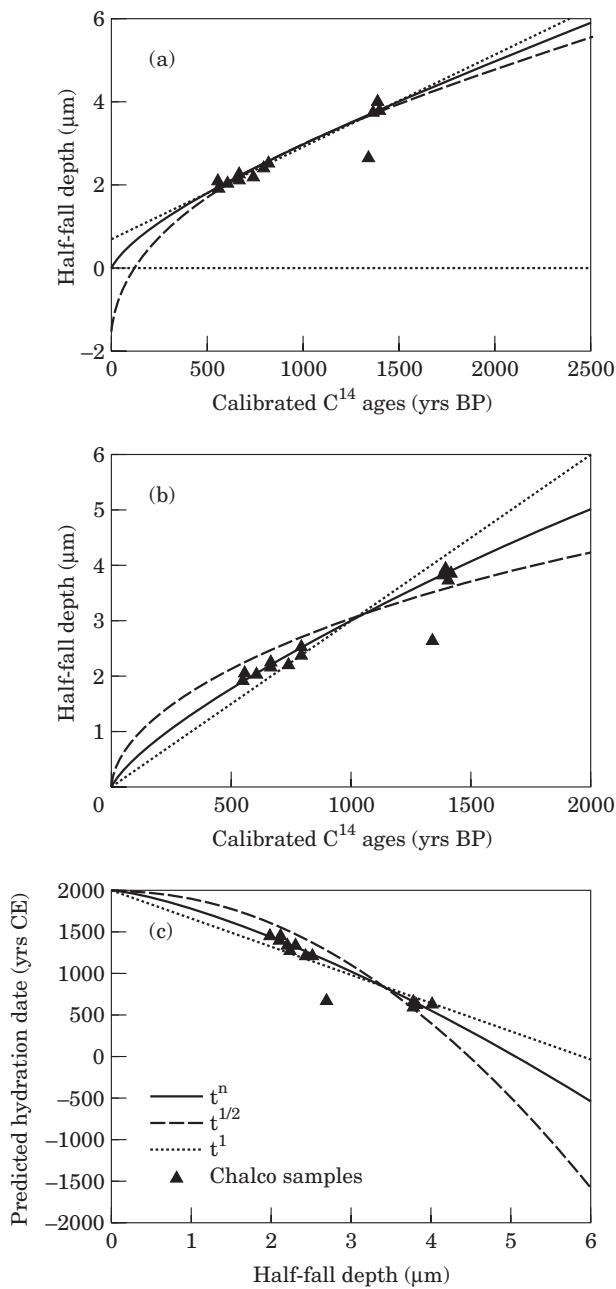


Figure 10. Plots of best fit half-fall depth calibration curves against <sup>14</sup>C ages for Chalco obsidian. (A) Calibration curves for t<sup>1</sup>, t<sup>1/2</sup>, and t<sup>n</sup> (n=0.757), where the depth at time zero is not constrained. Note that although all three curves could be used to correctly predict the ages of the Chalco samples, the t<sup>1/2</sup> curve intercepts the ordinate at a depth of -1.5 μm, and the t<sup>1</sup> curve requires a hydration depth of ~0.7 μm at zero time. (B) Calibration curves for t<sup>1</sup>, t<sup>1/2</sup>, and t<sup>n</sup> (n=0.757), where the constraint depth=0 at t=0 is imposed. Note the poor fit of both the t<sup>1/2</sup> and t<sup>1</sup> curves. (C) Calibration curves showing the relationship between half-fall depths and the predicted hydration age (in years CE) using the t<sup>1/2</sup>, t<sup>1</sup>, and t<sup>n</sup> (n=0.757) time relations. Note the increasing divergence at greater ages.

hydration age (Figure 11a, Table 5). The effects of using inappropriate rate models are illustrated in Figure 10c, wherein discrepancies become worse with

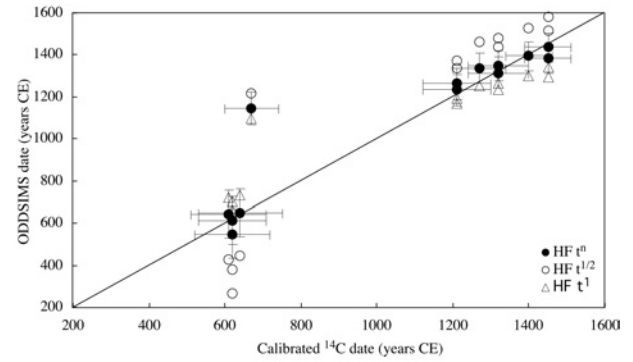


Figure 11 a

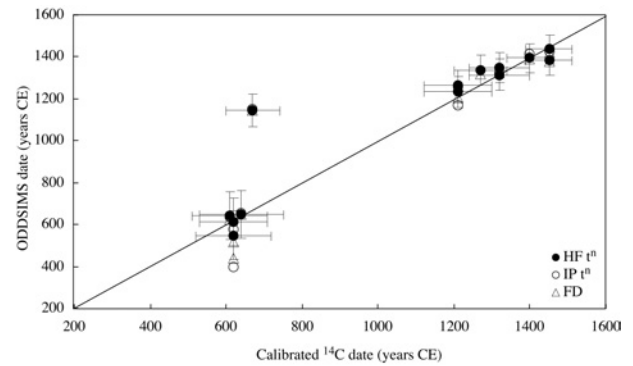


Figure 11 b

Figure 11. ODDSIMS ages plotted against associated <sup>14</sup>C dates. (A) Half-fall ages, calculated for the t<sup>n</sup> (n=0.757), t<sup>1/2</sup> and t<sup>1</sup> calibrations under the constraint that hydration depth is zero at zero time. Error bars are 1 standard deviation for the <sup>14</sup>C date, and error brackets resulting from a ± 0.1 to 0.15 μm in measured depth. For clarity, error bars are only plotted for the t<sup>n</sup> data. They will be similar for the other data. (B) Plot of ODDSIMS ages obtained using a t<sup>n</sup> calibration for different calibration points. HF—half-fall depth; IP—Inflection point depth; FD—Finite difference value.

increasing age, and very large errors in estimated age result. Therefore, we solved for the generalized t<sup>n</sup> equation (Model 3, equation 5). Even with the constraint that hydration depth must be zero at time zero, the generalized t<sup>n</sup> relationship fits the data very well (Figure 10a–c, 11a–b, Table 5) for all the characteristic point depths, and there is an excellent agreement between the derived half-fall dates and the <sup>14</sup>C dates. The coefficient (n) that is derived is probably an average of rates over the time range of the artifacts, and without testing over a broader time range should not be extrapolated, particularly for older samples. However, these results suggest that empirical ODDSIMS is promising if a generalized t<sup>n</sup> treatment is used. The empirical calibration curves could be used to date additional Pachuca obsidian at Chalco.

Inspection of the curves in Figure 10b and c suggests that the hydration data can be described by a t<sup>1/2</sup> relationship initially, followed by transition to a t<sup>1</sup> relationship. This possibility has been advocated previously (Meighan & Haynes, 1979; McGrail *et al.*,

Table 5. Summary of age results for SIMS analysis of Chalco samples

Sample	Calib. <sup>14</sup> C	SIMS HF t <sup>1/2</sup>	1σ	SIMS HF t <sup>1</sup>	1σ	SIMS HF t <sup>n</sup>	1σ	SIMS IP t <sup>n</sup>	1σ	Finite diff.	1σ	Max. wt% H <sub>2</sub> O
CHO110	1450	1580	70	1340	88	1436	70	1425	69	1422	59	1392
CHO110	1450	1518	72	1293	149	1382	71	1382	69	1376	59	1388
CHO086	1400	1531	72	1303	75	1394	71	1412	70	1390	63	1358
CHO081	1320	1480	74	1266	88	1351	72	1349	72	1350	68	1396
CHO081	1320	1437	76	1236	88	1315	73	1325	72	1322	68	1358
CHO120	1270	1461	75	1252	88	1335	72	1339	73	1318	73	1311
CHO015	1210	1371	78	1192	88	1262	74	1256	75	1260	78	1237
CHO018	1210	1334	80	1169	88	1233	75	1171	75	1206	79	1226
CHO047	640	444	133	730	110	650	114	657	84	651	117	621
CHO055	610	427	133	723	110	641	114	635	94	626	119	472
CHO051	620	267	138	659	110	549	118	399	94	440	119	451
CHO051	620	377	132	703	110	612	114	578	95	520	120	688
CHO030	670	1216	84	1098	88	1146	77	1149	84	1146	115	1092

All dates years CE. 1σ errors are estimated based on a conservative estimate of error associated with measuring crater depth ( $\pm 0.05\text{--}0.15\ \mu\text{m}$ , depending on crater depth), and are exclusive of errors associated with use of <sup>14</sup>C dates to calibrate the curve.

HF t<sup>1/2</sup>: date derived using SIMS half-fall depths (Table 2) fit to a t<sup>1/2</sup> relationship, assuming that x=0 at t=0.

HF t<sup>1</sup>: date derived using SIMS half-fall depths (Table 2) fit to a t<sup>1</sup> relationship, assuming that x=0 at t=0.

HF t<sup>n</sup>: date derived using SIMS half-fall depths (Table 2) fit to a t<sup>n</sup> (n=0.757) relationship, assuming that x=0 at t=0.

IP t<sup>n</sup>: date derived using SIMS inflection point depths (Table 2) fit to a t<sup>n</sup> (n=0.774) relationship, assuming that x=0 at t=0.

Finite difference: date derived using finite difference modeling of SIMS hydrogen depth profiles.

Max wt% H<sub>2</sub>O: date derived using the measured maximum water content in the profile, calibrated to a t<sup>n</sup> relationship.

1988; Garcia-Barcelona, 1989), and may help explain why attempts to empirically calibrate obsidian hydration rates using short-term experiments have failed. As illustrated in Figure 12, a relatively good calibration can be derived by fitting the general equation

$$x = k(Dt)^{1/2} + vt \quad (6)$$

where k and v are constants (Figure 12). This is essentially the same equation as the diffusion rate equation proposed by Wang *et al.*, (1969) for diffusion in glassy polymers. This treatment assumes that both the diffusion coefficient (D) and the surface concentration are constant, which are incorrect. However, the

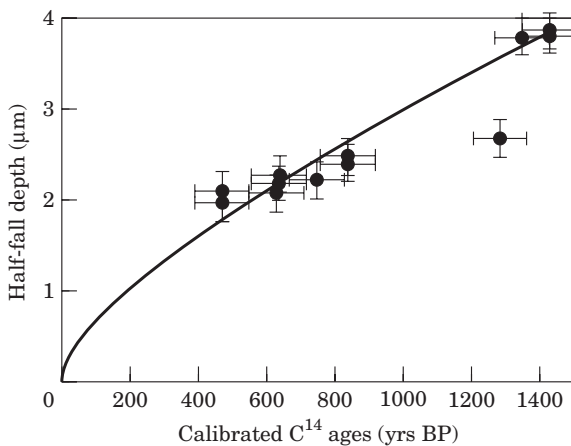


Figure 12. Curve of best fit obtained using an  $x = k(Dt)^{1/2} + vt$  relation regressed against half-fall depths of Chalco samples (assuming that at  $t=0$ ,  $x=0$ ). Similar relationships have been observed for diffusion in glassy polymers (Wang *et al.*, 1969).

relatively good agreement is intriguing, and suggests that there may be some similarities between diffusion in silicate glasses and polymers.

The major limitation to following the characteristic point approach outlined above is the dependency on a large number of <sup>14</sup>C dates, which may not always be available at a given site, or may be cost prohibitive to obtain. The possibility of using fewer samples to derive empirical curves can, however, be explored using our data set. In theory, only one sample is required (along with the condition that the hydration depth is zero at time zero), but the use of two samples provides greater control, particularly if the exponential (n) varies between sites or with time. The results in Table 6 indicate that very good agreement can be obtained between <sup>14</sup>C dates and half-fall dates for the Chalco samples using various pairs of samples, one each from the older and younger sample sets, to fit equation 5. Results using a number of obsidian pairs are very similar, and generally agree within 40 years of the half-fall ages obtained from regressions of all data. These results indicate that the empirical approach may be applied with minimum requirements for associated <sup>14</sup>C dates. The use of additional calibrations is optimal, both to improve confidence and as a check on the reliability of the obsidian sample—<sup>14</sup>C correlations (e.g., sample CHO030).

The ages obtained using the two types of characteristic points (half-fall and inflection point) to fit the <sup>14</sup>C dates are identical within error (Table 5, Figure 11). In most cases the two depths correlate extremely well, although the inflection point is slightly deeper. Each method has its advantages and disadvantages. Positive attributes for the inflection point include (1) the fact

Table 6. Results of two-point calibration half-fall ages for Chalco samples

Sample	Young sample Old sample <sup>14</sup> C date (CE)	CHO081 CHO051 date CE	CHO110 CHO051 date CE	CHO110 CHO047 date CE	CHO015 CHO047 date CE	SIMS t <sup>n</sup> (Table 3) date CE
CH0110	1450	1433	1447	1439	1427	1436
CH0110	1450	1379	1394	1385	1372	1382
CH0860	1400	1391	1406	1397	1383	1394
CH0081	1340	1348	1364	1354	1340	1351
CH0081	1340	1313	1328	1318	1303	1315
CH0120	1270	1332	1348	1338	1323	1335
CH0015	1210	1261	1277	1266	1250	1262
CH0018	1210	1233	1249	1237	1220	1233
CH0047	640	662	678	655	627	650
CH0055	610	653	669	646	617	641
CH0051	620	564	580	555	524	549
CH0051	620	671	688	665	636	612
CH0030*	670	1146	1163	1150	1131	1146

All calibrations used a young obsidian (<sup>14</sup>C age in the range of 1210–1450 CE), an old obsidian (<sup>14</sup>C age in the range 620–620 CE), and the constraint that the hydration depth is zero at time zero. The ages for the other obsidians not used to calibrate the curve are “independent” extrinsic hydration dates. SIMS t<sup>n</sup> is the age derived by the best fit to all samples.

that the inflection point is always in the middle of the steep section of the profile, and (2) there is no need to accurately measure the maximum hydrogen concentration, which may be effected by near-surface Na/K/H exchange. However, there are several disadvantages to the inflection point method. The inflection point measurements are all made at relatively low hydrogen concentrations, such that the counting statistical error over the depth of interest will be significantly larger than that of the half-fall depths. Thus, the inflection depth will be more sensitive to measurement uncertainties arising from analytical artifacts such as background hydrogen, surface roughness, and imperfect craters, as well as counting statistical limits. This sensitivity can be seen in the variability in inflection point dates obtained from replicate measurements for sample CHO051. Some of the advantages of using half-fall depths include (1) better counting statistical control, and (2) simplicity, such that results are available during the actual analysis. Also, the half-fall depth incorporates the maximum water content. Although it may be effected by near-surface cation exchange, the maximum water content appears to be time sensitive, and thus may be another monitor of the hydration rate. Thus, its use in the half-fall measurement means that two potential “clocks” are being utilized. For this sample set, there is almost no difference in ages derived using either type of characteristic point (Table 5), and it is obvious the either approach can be used to derive well-constrained ages. We will continue to assess the two characteristic points with additional samples from other sites.

#### Evaluation of maximum hydrogen concentration as a potential chronometer

The correlation between sample age and maximum hydrogen concentration (Figure 7) suggests that this

detail of the SIMS profile may also potentially contain age information. These analyses were not optimized to maximize the precision of this measurement but, nevertheless, can be used to at least estimate the potential of the method. The maximum hydrogen content was regressed with sample age. The calibration provides “hydrogen content” dates that are in relatively good agreement (within 100 years) with ages determined using <sup>14</sup>C or half-fall depths, using a t<sup>n</sup> relation (Figure 13, Table 5). These results suggest that this approach warrants further investigation, as it has two potential advantages. First, this calibration is independent of whatever errors are associated with the measurement of the depth of the SIMS sputter crater, because only the maximum hydrogen concentrations are used. In addition, this approach requires significantly less analytical time because the peak hydrogen concentration is encountered early in the profile. At the very least, this approach may provide another check on the date

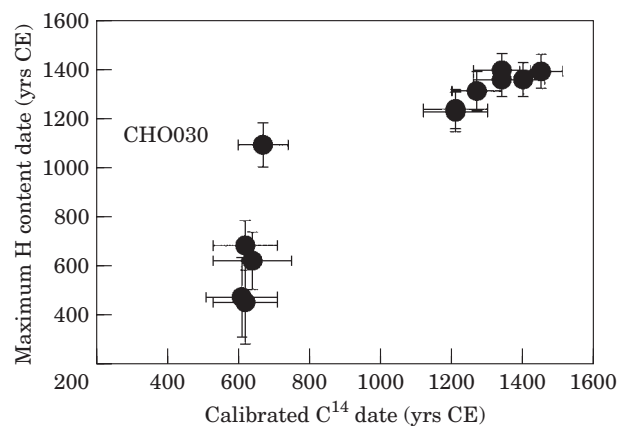


Figure 13. Plot of ages obtained using the maximum hydrogen content in each profile against <sup>14</sup>C ages.

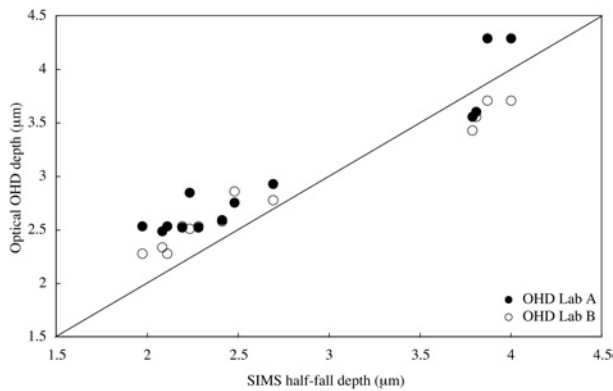


figure 14

Figure 14. Plot of half-fall depth measured using SIMS against the “half-fall” depth measured using optical techniques in two different laboratories. Stated errors are smaller than the symbol size.

determined from the concentration profile, and/or provide information on site-specific environmental conditions.

#### Comparison with intrinsic OHD dates

As summarized earlier, the application of intrinsic OHD to Chalco obsidian artifacts resulted in dates in gross disagreement with all other contextual information. Comparison of the results of SIMS analyses with the optical measurements on the same samples allows some evaluation of this problem. There is a general correlation between SIMS half-fall depths and optical data from OHD Labs A and B, although optical OHD depths are systematically deeper than SIMS half-fall depths (Figure 14). However, there is much greater scatter in the OHD depths, which is not surprising given the measurement uncertainties outlined in Anovitz *et al.* (1999). Of even greater concern is the discrepancy in depths measured on the same artifacts in two different laboratories, which are as large as 0.8 µm. Variation in depths of a few tenths of a micron can result in age differences of hundreds of years depending on the absolute age of the sample (Figure 11). The absolute calibration is also seriously flawed, as OHD ages are systematically older than the  $C^{14}$  ages, with discrepancies of over 1000 years in some samples (Figure 15). Although applying an empirical calibration with  $^{14}C$  dates to the optical data removes the large and systematic age discrepancy, it does not eliminate the large scatter in derived ages arising from errors in the actual depth measurement.

#### The anomalous date for CHO030—an explanation

Specimen CHO030 was recovered from level 12 of excavation Unit A, and the radiocarbon assay (see Table 1) produced a calibrated (2 sigma) range of 600–820 CE with an intercept of 670 CE. Additionally, the majority of diagnostic sherds recovered were

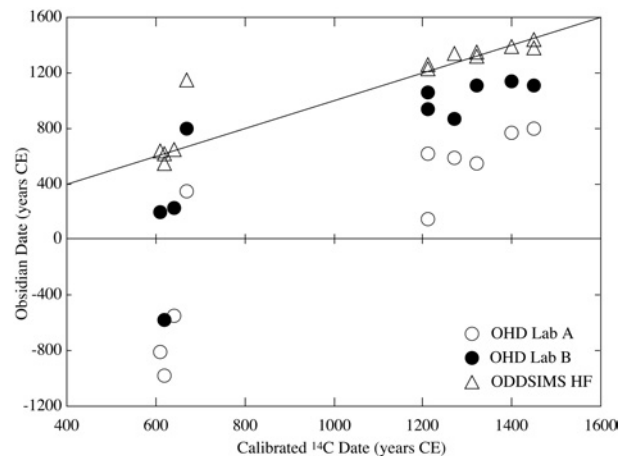


Figure 15. Plot of half-fall ages obtained using ODDSIMS and optical OHD from two different labs, compared to associated  $^{14}C$  dates.

Epiclassic, a result that corroborates the radiocarbon assay (see Hodge, *in press*). However, the SIMS analysis indicated that this artifact is considerably younger and probably dates to the beginning of the second occupation (Early Postclassic). During the excavation of Mound 65, a number of rodent burrows containing artifacts were identified, and it is possible that CHO030 is a younger artifact which fell into an older deposit. Additional evidence supporting this interpretation is found in the fact that CHO030 is made of Pachuca obsidian and was recovered from a level that primarily produced artifacts made with Otumba obsidian (Elam, *in press*; Elam *et al.*, *in press*). The pattern of source utilization at Mound 65 indicates substantially greater use of Otumba than Pachuca obsidian during the Epiclassic. During the Postclassic (Aztec periods) this pattern is reversed. Further evidence supporting a Postclassic date for this piece is observed in the artifact’s morphology. CHO030 is the medial portion of an irregular blade and although it lacks the proximal end which might provide a more definitive typological indicator of age, this form is more typical of that found in the Early Aztec levels of Mound 65.

#### Finite Difference Modelling—Towards an Intrinsic Method

While characteristic point models based on either half-fall distances or inflection points have obvious utility for locally calibrated dating, they are limited because they do not directly model submicroscopic processes in the obsidian during diffusion. Thus, it is unlikely they can be used to create a universal, intrinsic model. A more rigorous approach requires direct modelling of the diffusion process. Such an approach needs to be tied to the microstructural processes occurring during hydration so that the effects of changing compositional or environmental variables can be

incorporated. In our previous work (Anovitz *et al.*, 1999) we showed that a finite difference model had the potential for such an application, in that it was capable of reproducing the detailed shape of the hydrogen concentration depth profiles measured in real obsidians.

The finite difference method uses a numerical calculation to model the formation of the entire diffusion profile as a function of time, and is fit to the profile as a whole (excluding the near-surface region). Solution of the equations involves a number of assumptions, including boundary conditions and the nature of the actual diffusion process so that appropriate diffusion equations can be selected. This technique is substantially more complex than the characteristic point approach. However, the goodness of fit to the measured profile provides a method of evaluating whether the choice of diffusion equation (and hence mechanism) is appropriate, yielding insights into the actual process of hydration that are not available using “characteristic point” techniques. Below, we will extend this model to reproduce the results from the Chalco sample suite, laying the foundation for further work on developing an intrinsic age dating technique.

*Model characteristics.* Nearly all diffusion problems require derivation of a solution to one of Fick’s Laws. For situations like obsidian hydration, where the concentration is known as a function of distance, this involves solution of Fick’s second law:

$$\frac{\partial C}{\partial t} = \frac{\partial}{\partial x} D \frac{\partial C}{\partial x} \quad (7)$$

which describes changes in concentration (C) with time (t) and distance (x) as a function of a diffusion coefficient (D). This equation can only be simplified to the more common form:

$$\frac{\partial C}{\partial t} = D \frac{\partial^2 C}{\partial x^2} \quad (8)$$

if D is not a function of depth within the sample. As hydrogen concentration varies with depth, this is equivalent to D being independent of concentration. However, the shape of the hydration profile indicates that this is not the case, and that this simplification is inappropriate (Anovitz *et al.*, 1999).

Anovitz *et al.* (1999) showed that, with an appropriate choice of an equation for D and ignoring near surface effects which may be related to interdiffusion of hydrogen and alkali elements, equation (7) can be used to describe the hydrogen diffusion profiles observed in obsidian. However, the equation used for D was empirical, and thus does not explicitly describe the microstructural processes involved. Most importantly, as noted above, available evidence suggests that it is hydrogen, not water that diffuses into the glass. In the glass structure, infrared (IR) data suggest that hydro-

gen is present both as relatively immobile hydroxyl groups and more mobile molecular water, the relative proportions of which change with total hydrogen concentration and temperature. Following Crank (1975) and Doremus (1995), but retaining the concentration dependence of D, equation (7) can be expanded to allow for the reaction between the water or hydrogen and silicate framework as follows:

$$\frac{\partial C}{\partial t} = \frac{\partial}{\partial x} D \frac{\partial C}{\partial x} - \frac{\partial S}{\partial t} \quad (9)$$

where C is now the concentration of the mobile component (molecular water) and S the concentration of the immobile or sink component (OH). If necessary, this can be further modified to allow for some OH mobility and OH/H<sub>2</sub>O exchange kinetics. Unfortunately, other types of information are required to calibrate such a model. As noted by Crank (1975), however, this approach is mathematically identical to that described by equation (7). Thus, equation (7) can be used as a proof of the approach until additional experimental data are available.

Solution of equation (7) is non-trivial. Few analytical solutions exist for any choice of equations for D described in Crank (1975). A finite difference solution, a standard method for numerical solution of differential equations, was therefore adopted. Given pre-defined initial and boundary conditions, this provides a series of solutions at discrete distances and times. Intermediate values are not defined, but can be approximated by interpolation if needed.

The general finite-difference solution for equation (7), assuming variable distances between the spatial nodes, and re-arranging to solve for the concentration at a given node, is:

$$C_i^{t2} = \frac{\left( C_i^{t1} + 2D_i \Delta t \left( \frac{C_{i+1}}{\Delta x_i \Sigma x} + \frac{C_{i-1}}{\Delta x_{i-1} \Sigma x} \right) + \Delta t \left( \frac{D_{i+1} - D_{i-1}}{\Sigma x} \right) \left( \frac{C_{i+1} - C_{i-1}}{\Sigma x} \right) \right)}{B} \quad (10)$$

where

$$B = 1 + \frac{2D_i \Delta t}{\Delta x_i \Delta x_{i-1}}$$

and x is the distance from the surface, so that:

$$\Delta x_i = x_{i+1} - x_i$$

$$\Sigma x = \Delta x_i + \Delta x_{i-1}$$

The superscripts refer to the time step, and the subscripts to the node. The length of the time step is  $\Delta t$ ,  $C_i$  is the concentration at a given node, and  $D_i$  is the diffusion coefficient appropriate to the concentration at

the  $i$ th node. As this equation is algebraic, its solution appears trivial. There are, however, complications. Equation (10) contains a simplification of the finite difference solution to the second derivative for non-constant inter-node distances, although work is ongoing to refine this solution. Additionally, equation (10) does not define what timestep should be used for each value of the concentration at a given node. There are two end-member approaches to this problem. In explicit finite difference modelling the values at timestep  $(t+1)$  are based on values at timestep  $(t)$ . This is the simplest approach because the starting values at timestep  $(t=0)$  are pre-determined and values for each succeeding timestep can be calculated directly. Unfortunately, for some combinations of  $D$ ,  $\Delta t$  and  $\Delta x$  an explicit solution becomes numerically unstable.

The alternative is the implicit finite difference approach. In this case the values of the concentrations at timestep  $(t)$  are based on concentrations at timestep  $(t+1)$ , and must be obtained by iteration. It is assumed initially that the concentrations at timestep  $(t+1)$  are equal to those at timestep  $(t)$ . Once a solution is obtained the newly calculated values are used to obtain a second estimate. This is repeated until the result is stable. Implicit finite difference calculations are unconditionally stable, but the iterations require greater calculation time. A third alternative utilizes a weighted average of the explicit and implicit approaches. In the Crank-Nicholson method (Crank, 1975) the average of the two is used. In our calculations this occasionally yielded some numerical instability due to the large initial difference between the initial hydrogen concentration values at the first (surface) and second (baseline) nodes. A fully implicit approach was therefore adopted.

The finite difference model has been written to allow for variable  $\Delta x$  and  $\Delta t$  values. The grid spacing ( $\Delta x$ ) varies, with the nodes being spaced more closely near the glass surface. This provides detailed information near the surface where the actual diffusion profile forms, but a long enough total distance that, for the calculations of interest, the system acts as a one-dimensional, semi-infinite medium and a no-flow boundary condition can be imposed at depth. The initial time steps are quite short. Initially a significant discontinuity can exist between the surface boundary value, assumed in some calculations to be constant at the hydrogen surface concentration, and the first node, assumed initially to equal the baseline hydrogen concentration. Short initial time steps enhance the numerical stability of the model. Once this initial instability is overcome, however, it becomes possible to increase  $\Delta t$  (values up to two years were used) to decrease calculation time.

**Modeling procedure and results.** The SIMS data for the Chalco samples exhibits several features which needed to be incorporated into the final model. First, and most significant, the overall profile is S-shaped. This dictates

the use of a concentration-dependent or diffusion/reaction model (Anovitz *et al.*, 1999; as noted by Crank, 1975 these are mathematically equivalent). Second, the surface concentration appears to change as a function of time. Figure 6 shows that younger samples, in addition to having narrower profiles, also have lower maximum water contents. This suggests that the surface concentration does not equilibrate immediately (or may never equilibrate). While the near-surface effects of Na/K diffusion (and adsorbed H) do not allow the surface concentration to be measured directly, a model of the process requires this change to be accounted for. Third, the background water concentration for each profile appears to be slightly different. This may be real, or due to analytical uncertainties, but the differences are small and an averaged value can be used for global modelling. In spite of these problems, the temporal correlation with both surface concentration and the depth of each profile suggest that creation of a generalized finite difference model is possible.

The following procedure was adopted in modelling these data. First, the profile from CHO055 was chosen and modeled using the average baseline hydrogen concentration and assuming a constant surface concentration, which was adjusted to yield a best fit to the data. We adopted an equation for  $D$  as a function of concentration of the form:

$$D = D_0 \cdot (1 + (x \cdot C)^y) \quad (11)$$

following Anovitz *et al.* (1999). In this equation  $D_0$  primarily effects the depth of the profile at a given time. The variables  $x$  and  $y$  control the shape of the profile but also modify the rate of profile growth. The fitting procedure involved calculating the profiles developed in the glass as a function of time to 1600 years, then calculating the chi squared value for each time step relative to the measured profile, exclusive of the near-surface region. The minimum in the chi squared versus time curve was then chosen as the best fit. This was repeated, varying each parameter independently, until both a satisfactory fit and age were achieved. This yielded:  $D_0 = 2.531 \times 10^{-13}$  microns<sup>2</sup>/sec,  $x = 1.6$ ,  $y = 2.51$ . These parameters were used to obtain a best fit for each of the other profiles, varying only the surface and background concentration levels.

The surface values as a function of time for each profile were then fit to the function:

$$C_{\text{surf}} = C_e^* (2 - C_a^* \exp(-tC_d) - (2 - C_a^*) \cdot (\exp(-tC_b))) \quad (12)$$

This equation yields a surface concentration which initially increases rapidly, then flattens as the equilibrium value is approached (Figure 16). The  $C_e$  coefficient is half the equilibrium value and it and  $C_d$  are derived by regression from the Chalco samples whose surface values were fitted in the previous step. The

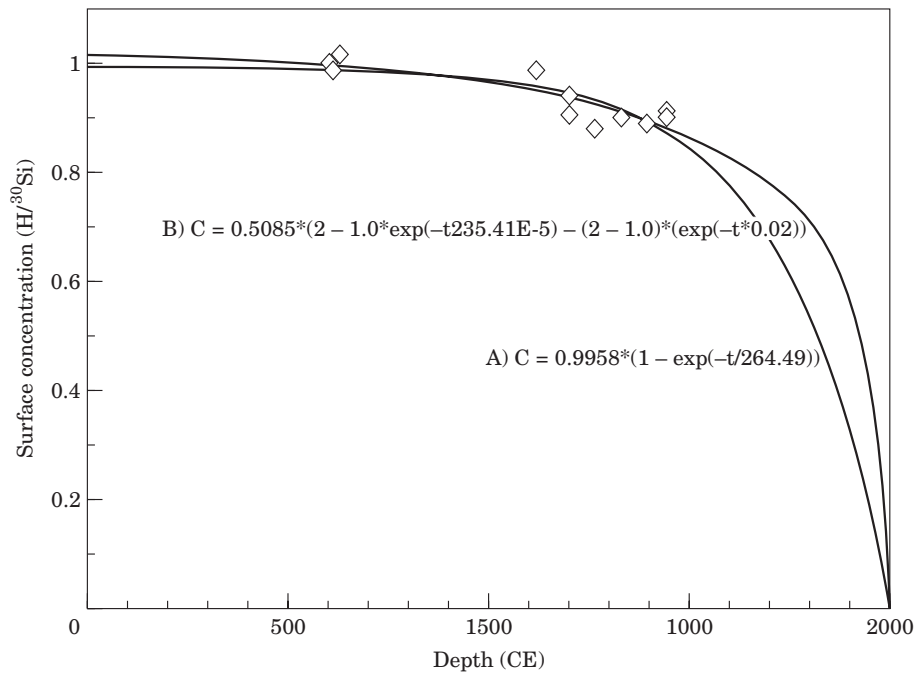


Figure 16. Fitted surface concentrations and model values for surface water concentration as a function of time using the finite difference model for three Chalco samples.

coefficient  $t$  is time, and  $C_a$  and  $C_b$  control the initial hydration rate: the larger  $C_b$ , the faster the initial increase in water content (from  $t=0$ ); the smaller  $C_a$ , the sharper the transition from the initial, rapidly increasing part of the curve to the flatter, near equilibrium section. Unfortunately, testing demonstrated that the initial shape of the profile has a profound effect on the relative rate of growth of the profile with time, and the youngest sample ( $\sim 600$  years old) is too old to provide strong constraints on the initial shape of the profile. The model calculation was therefore repeated, modelling all of the sample profiles simultaneously assuming an average background value of 0.0473 and surface values that varied with time according to the above equation. The relative growth rate of the profile with time was then varied by changing  $C_a$  or  $C_b$ , refitting the other parameters in equation (12) to the sample data, adjusting  $D_0$  as needed, and repeating the process until a best fit to the  $^{14}\text{C}$  ages was achieved. This yielded:  $C_c=0.5085$ ,  $C_a=1.0$ ,  $C_b=0.02$ , and  $C_d=232.41 \times 10^{-5}$ .

Two samples were excluded from the finite difference modelling, and are not included in the statistical analysis that follows. As previously discussed, qualitative examination of CHO030 suggests that it has been stratigraphically relocated, possibly due to rodent activity. One of the analyses on sample CHO051 (2) was also excluded, as the profile has a significantly different shape compared to the other profiles, possibly due to roughness on the analysed surface. Although it is a poor candidate for fitting with a generalized model, reasonable ages can still be obtained from this profile by characteristic point analysis.

Calculated profiles from the final, integrated model for three Chalco samples covering a range of times illustrate the excellent agreement between the model and actual profiles at depths from the maximum hydrogen concentration to the background value (Figure 17). As the near-surface features are not a component of this model, they are not reproduced, but the overall results are very encouraging. Figure 16 shows the surface concentration versus time model used in these calculations. Curve A is a best fit to the available data, which suggests a fairly slow initial surface hydration. This seems unlikely, as the exposed glass surface should begin to hydrate rapidly on exposure. SIMS analysis of obsidian hydrated for only 15 years at temperatures as low as  $10^\circ\text{C}$  indicates that the surface already has high water contents (Riciputi *et al.*, in submission). Not surprisingly, this model generates ages for the youngest samples that are too old. The best fit (Curve B) generates the model ages listed in Table 3 and shown in Figure 11, which are quite consistent with the  $^{14}\text{C}$  ages. Younger samples from the colonial period would be of great assistance in fixing the appropriate shape of the curve in Figure 16.

## Conclusions and Future Directions

This results of this study suggest that the use of hydrogen concentration depth profiles measured by SIMS may provide data of sufficient quality to allow the use of obsidian hydration for accurate and precise age dating. Both the depth of the hydration profile and the maximum water content are well-correlated with

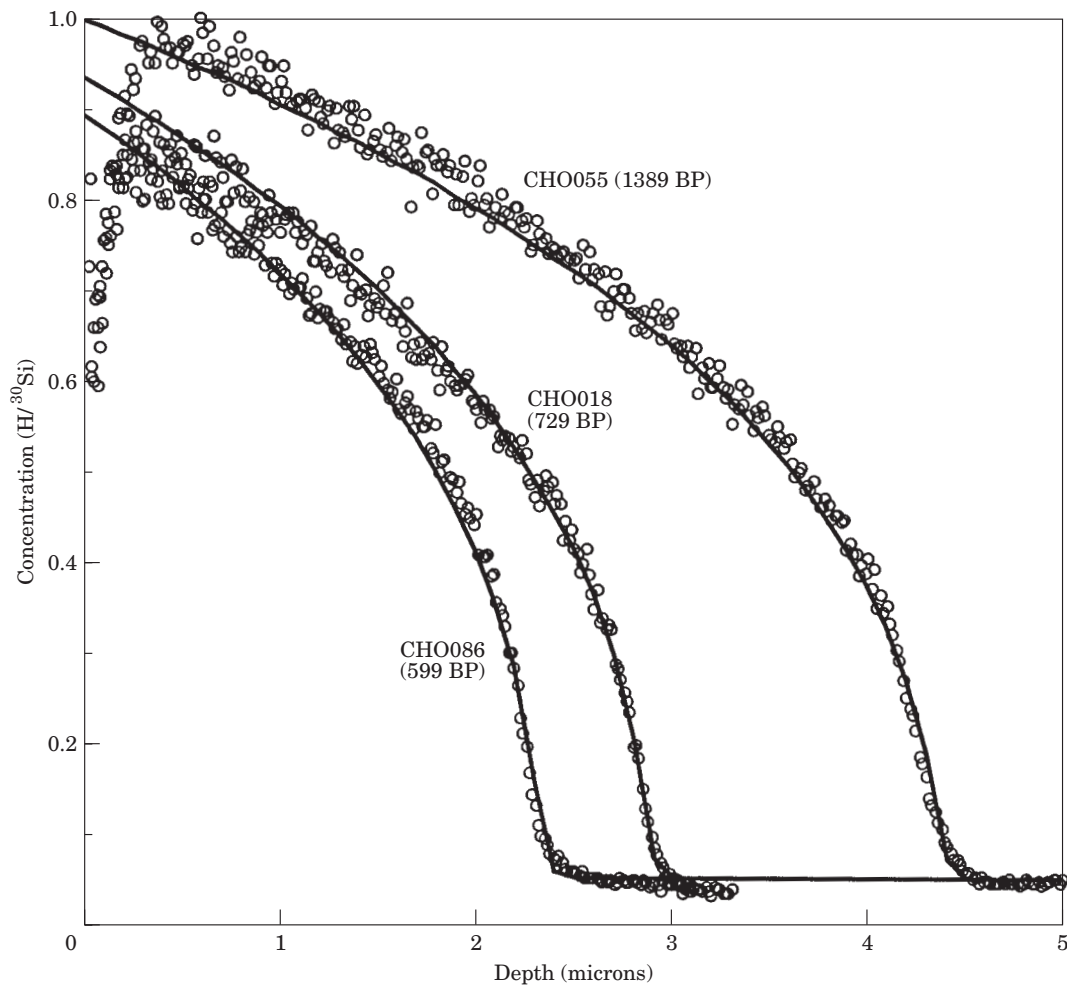


Figure 17. Examples of the fit of the finite difference model to hydrogen profiles from three Chalco samples.

age, providing multiple methods of dating. These results confirm that hydration rates are concentration dependent, and are not linear with either a  $t^1$  or  $t^{1/2}$  time-depth relationship. However, solving for the general equation  $t^n$  by regressing depth against  $^{14}\text{C}$  ages for a suite of obsidian artifacts from Chalco indicates that an excellent correlation can be achieved, suggesting that using characteristic points may yield excellent results for empirical studies. This is confirmed by the successful results obtained using  $^{14}\text{C}$  dates from just two artifacts, and the constraint that hydration depth is zero at time zero, to calibrate the depth-age curve, and then using this curve to derive ages for the other artifacts. These extrinsic ODDSIMS ages agree very well with the  $^{14}\text{C}$  ages, and indicate that the method can be quite successful if there are a few artifacts with associated  $^{14}\text{C}$  dates available at a site.

If a predictive, uncalibrated, intrinsic approach is to be developed, additional refinements are still needed. This work shows that the finite difference approach can reproduce the observed time vs. depth progression as well as characteristic point models. The finite difference

equations are based on a number of assumptions about the behavior of water as it diffuses into the glass. The good agreement between the measured and predicted profile shapes suggests that the basic assumptions are correct. However, a number of parameters will have to be rigorously quantified before the potential of an intrinsic approach can be fully evaluated. The model will have to explicitly account for the reaction of water with the silicate framework to form OH and  $\text{H}_2\text{O}$  (or, for that matter,  $\text{H}_2$  or  $\text{H}_3\text{O}^+$ ) as well as the kinetics of this process. The effects of changes in the composition of the glass and the nature of the reaction at the glass/water interface will also have to be understood. This has become a standard approach for analysis of the reaction of water with high-temperature silicate glasses or melts (cf. Zhang *et al.*, 1991, 1995; Doremus, 1999), and provides an avenue for generalization of ODDSIMS. Temperature (and potentially relative humidity) control will have to be developed, and depending on the sensitivity of the model to these parameters, techniques to constrain these values for archaeological samples will have to be evaluated. In addition, if other

obsidian sources are to be used, the effects of major element composition on hydration rates will have to be investigated.

The processes which cause the near-surface changes in the hydration profile may also provide important information allowing further quantification of temporal effects. These processes may be related to alkali exchange (Anovitz *et al.*, 1999). Examination of the Chalco data suggests that, in the very near surface, hydrogen diffusion is an uphill process, against the changing water concentration gradient. This implies that the thermodynamics of mixing of the glass, water and other diffusing elements are strongly nonideal. Such processes are not unknown (cf. Crank, 1975), but imply that the thermochemistry of the multicomponent diffusion process is somewhat complex (the cross terms in the multicomponent diffusion matrix must be nonzero).

In spite of these complications, the very simple characteristic point analysis indicates that the hydration rate at a single site can be very systematic with time, and that the complex hydration mechanism may be reduced to allow successful empirical modelling of hydration rate-time dependencies. The SIMS method provides excellent precision and accuracy, and outside of the uncertainties inherent in the  $^{14}\text{C}$  calibration, is mainly limited by errors associated with measurement of the crater depth. Although the depth errors vary with surface roughness and crater depth (age), for artifacts of 500–1500 years in age, the analytical errors translate into two standard errors on the order of 50–100 years, similar to the precision available from  $^{14}\text{C}$  age dating. In addition, the ODDSIMS technique provides a direct measurement of the age of the artifact itself, avoiding potential association errors that can be problematic with carbon dating (e.g., sample CHO030). These results indicate that, although a great deal of work remains to be done, the ODDSIMS technique holds considerable potential as a tool to date obsidian artifacts, and that this may finally provide the method to realize the potential of hydration dating.

## Acknowledgements

Research sponsored by the Division of Chemical Sciences, Geosciences and Biosciences, Office of Basic Energy Sciences, U.S. Department of Energy under contract DE-AC05-00OR22725 with Oak Ridge National Laboratory, managed by UT-Battelle LLC, and by National Science Foundation grant SBR-98-04350 and BCS-0108956 to the University of Tennessee. We also thank the Instituto Nacional de Antropología e Historia (INAH), especially Ing. Joaquin Garcia-Barcena, Presidente de Consejo de Arqueología, INAH for his advice and assistance. We thank Richard Klein and two anonymous reviewers, whose suggestions greatly improved the manuscript. Finally, we would like to acknowledge the late Dr

Mary Hodge who provided the Chalco obsidian sample set. Her careful work, both in the field and in the lab, made the analysis presented here possible. It is to her memory that we dedicate this report.

## References

- Aitkin, M. J. (1997). *Science-based Dating in Archaeology*. London & New York: Longman Archaeology Series.
- Ambrose, W. R. (1976). Intrinsic hydration rate dating of obsidian. In (R. E. Taylor, Ed.) *Advances in Obsidian Glass Studies*. New Jersey: Noyes Press, pp. 81–105.
- Anovitz, L. M., Elam, J. M., Riciputi, L. R. & Cole, D. R. (1999). The Failure of Obsidian Hydration Dating: Sources, Implications and New Directions. *Journal of Archaeological Science* **26**, 735–752.
- Braswell, G. E. (1992). Obsidian hydration dating, the Coner phase and revisionist chronology at Copan, Honduras. *Latin American Antiquity* **3**, 130–147.
- Braswell, G. E., Glascock, M. D. & Neff, H. (1996). The obsidian artefacts of Group 10L-2, Copan: production, exchange and chronology. Paper Presented at the 61st Annual Meeting of the Society for American Archaeology, New Orleans, LA, April 1996.
- Charlton, T. H., Nichols, D. L. & Charlton, C. O. (1991). Aztec craft production and specialization: archeological evidence from the city-state of Otumba, Mexico. *World Archaeology* **23**, 98–114.
- Crank, J. (1975). *The Mathematics of Diffusion*. Oxford: Oxford University Press.
- Doremus, R. H. (1995). Diffusion of water in glass. *Journal of Materials Research* **10**, 2379–2389.
- Doremus, R. H. (1999). Diffusion of water in rhyolite glass: Diffusion-reaction model. *Journal of Non-crystalline Solids* **261**, 101–107.
- Elam, J. M. (1993). *Obsidian exchange in the Valley of Oaxaca, Mexico 2500–500 BP*. Ph.D. Thesis. University of Missouri-Columbia, Columbia, MO.
- Elam, J. M. (in press). Style and use of obsidian and other lithic artifacts. In (M. Hodge, Ed.) *Place of Jade: Society and Economy in Ancient Chalco*. Pittsburgh, PA: Monographs in Latin American Archaeology, University of Pittsburgh.
- Elam, J. M., Glascock, M. D. & Neff, H. (1994). Obsidian artifacts from Oaxaca, Mexico: source identification and hydration dating. In (D. A. Scott & P. Meyers, Eds) *Archaeometry of Precolumbian Sites and Artifacts*. Los Angeles, CA: Getty Conservation Institute, pp. 135–160.
- Elam, J. M., Glascock, M. D. & Neff, H. (in press). Obsidian source analysis. In (M. Hodge, Ed.) *Place of Jade: Society and Economy in Ancient Chalco*. Pittsburgh, PA: Monographs in Latin American Archaeology, University of Pittsburgh.
- Friedman, I. & Long, W. (1976). Hydration rate of obsidian. *Science* **191**, 347–352.
- Friedman, I. & Smith, R. (1960). A new method of dating using obsidian: Part I, the development of the method. *American Antiquity* **25**, 476–522.
- Friedman, I., Smith, R. L. & Long, W. D. (1966). Hydration of natural glass and formation of perlite. *Geological Society of America Bulletin* **77**, 232–327.
- García-Barcena, J. (1989). Las Ecuaciones de Hidratación de la Obsidiana. In (G. M. Gaxiola & J. E. Clark, Eds) *La Obsidiana en Mesoamérica*. Mexico: Colección Científica, Serie Arqueología, Instituto Nacional de Antropología e Historia, pp. 59–68.
- García de Miranda, E. (1987). *Modificaciones al Sistema de Clasificación Climática de Köppen (para adaptarlo a las condiciones de la República de México)*. Mexico: Instituto Nacional de Estadística y Geografía, p. 135.
- Geyh, M. A. & Schleicher, H. (1990). *Absolute Age Determination*. Berlin: Springer-Verlag.

- Grun, R. (1997). Electron Spin Resonance Dating. In (R. E. Taylor & M. J. Aitken, Eds) *Chronometric Dating in Archaeology*. Advances in Archaeological and Museum Science, Vol. 2. New York and London: Plenum Press, pp. 217–260.
- Hodge, M. G. (in press). *Place of Jade: Society and Economy in Ancient Chalco*. Pittsburgh, PA: : Monographs in Latin American Archaeology, University of Pittsburgh.
- Lee, R. (1969). Chemical temperature integration. *Journal of Meteorology* **8**, 423–430.
- McGrail, B. P., Pederson, L. R., Strachan, D. M. & Ewing, R. C. (1988). Obsidian hydration dating—field, laboratory and modeling results. *Materials Research Society Symposium Proceedings* **123**, 263–269.
- Meighan, C. W. & Haynes, C. V. (1970). The Borax Lake site revisited. *Science* **167**, 1213–1221.
- Michels, J. W., Tsong, I. S. T. & Smith, G. A. (1983). Experimentally derived hydration rates in obsidian dating. *Archaeometry* **25**, 107–117.
- Neff, H., Bove, E. J., Johnson, T. H. & Arroyo, B. (1993). Fechimientos a traves de hidratacion de obsidiana en la costa sur de Guatemala. *Apuntes Arqueologicos* **2**, 55–79.
- Nichols, D. L. & Charlton, T. H. (1996). The postclassic occupation at Otumba. *Ancient Mesoamerica* **7**, 231–244.
- Parsons, J. R., Brumfiel, E. M., Parsons, H. & Wilson, D. J. (1982). *Prehistoric Settlement Patterns in the Southern Valley of Mexico: The Chalco-Xochimilco Regions*. Ann Arbor, MI: Memoirs No. 14, Museum of Anthropology, University of Michigan.
- Riciputi, L. R., Anovitz, L. M. & Elam, J. M. (in submission). SIMS analysis of Wekwok obsidian under ambient conditions: Implications for temperature dependence of obsidian hydration rates. *Geoarchaeology*.
- Ridings, R. (1996). Where in the world does obsidian hydration dating work? *American Antiquity* **61**, 136–148.
- Sanders, W. T., Parsons, J. R. & Santley, R. S. (1979). *The Basin of Mexico: Ecological Processes in the Evolution of a Civilization*. New York, NY: Academic Press.
- Santley, R. S., Kerley, J. M. & Kneebone, R. R. (1986). Obsidian working, long distance exchange and the politico-economic organization of early states in Central Mexico. In (B. L. Issacs, Ed.) *Research in Economic Anthropology, Supplement 2*. Greenwich, CT: JAI Press, Inc., pp. 101–132.
- Stark, B. L., Heller, L., Glascock, M. D., Elam, J. M. & Neff, H. (1992). Obsidian-artifact analysis for the La Mixtequilla region, South-Central Vera Cruz, Mexico. *Latin American Antiquity* **3**, 221–239.
- Stevenson, C. M., Carpenter, J. & Scheetz, B. E. (1989). Obsidian dating: Recent advances in the experimental determination and application of hydration rates. *Archaeometry* **31**, 1193–1206.
- Stevenson, C. M., Mazer, J. J. & Scheetz, B. E. (1998). Laboratory Obsidian Hydration Rates. Theory, Method and Application. In (M. S. Shackley, Ed.) *Archaeological Obsidian Studies. Method and Theory*. New York, NY: Plenum Press, Advances in Archaeological and Museum Science, Vol. 3, pp. 181–204.
- Wang, T. T., Kwei, T. K. & Frisch, H. L. (1969). Diffusion in glass polymers III. *Journal of Polymer Science* **7**, 2019–2028.
- Webster, D. & Freter, A. (1990). Settlement history and the Classic collapse at Copan: a redefined chronological perspective. *Latin American Antiquity* **1**, 66–85.
- Zhang, Y., Stolper, E. M. & Wasserberg, G. J. (1991). Diffusion of water in rhyolitic glasses. *Geochim Cosmochim Acta* **55**, 441–456.
- Zhang, Y., Stolper, E. M. & Ihinger, P. D. (1995). Kinetics of the reaction  $H_2O+O=2OH$  in rhyolitic and albitic glasses: preliminary results. *Amer Mineral* **80**, 593–612.